

Supersymmetry discovery potential of the LHC at $\sqrt{s} = 10$ and 14 TeV without and with missing E_T

Howard Baer^a, Vernon Barger^b, Andre Lessa^a and Xerxes Tata^c

^a*Dept. of Physics and Astronomy, University of Oklahoma, Norman, OK 73019, USA*

^b*Dep't of Physics, University of Wisconsin, Madison, WI 53706, USA*

^c*Dept. of Physics and Astronomy, University of Hawaii, Honolulu, HI 96822, US*

E-mail: baer@nhn.ou.edu, barger@physics.wisc.edu, lessa@nhn.ou.edu, tata@phys.hawaii.edu

ABSTRACT: We examine the supersymmetry (SUSY) reach of the CERN LHC operating at $\sqrt{s} = 10$ and 14 TeV within the framework of the minimal supergravity model (mSUGRA). We improve upon previous reach projections by incorporating updated background calculations including a variety of $2 \rightarrow n$ Standard Model (SM) processes. We show that SUSY discovery is possible even before the detectors are understood well enough to utilize either E_T^{miss} or electrons in the signal. We evaluate the early SUSY reach of the LHC at $\sqrt{s} = 10$ TeV by examining multi-muon plus ≥ 4 jets, and also lepton-free, acollinear dijet events with *no* missing E_T cuts, and show that the greatest reach in terms of $m_{1/2}$ occurs in the dijet channel, where it may be possible to probe $m_{\tilde{q}} \sim m_{\tilde{g}} \lesssim 1$ TeV with just 1 fb^{-1} of integrated luminosity. The reach in multi-muons is slightly smaller in $m_{1/2}$, but extends to higher values of m_0 . We find that an observable multi-muon signal will first appear in the opposite-sign dimuon channel, but as the integrated luminosity increases the relatively background-free but rate-limited same-sign dimuon, and ultimately the trimuon channel yield the highest reach. The optimized reach in these channels extends to $m_{\tilde{g}} \lesssim 600$ (800) GeV for an integrated luminosity of 100 pb^{-1} (1 fb^{-1}). We show characteristic distributions in these channels that serve to distinguish the signal from the SM background, and also help to corroborate its SUSY origin. We then evaluate the LHC reach in various no-lepton and multi-lepton plus jets channels *including* missing E_T cuts for $\sqrt{s} = 10$ and 14 TeV, and plot the reach for integrated luminosities ranging up to 3000 fb^{-1} at the SLHC. For $\sqrt{s} = 10$ TeV, the LHC reach extends to $m_{\tilde{g}} = 1.9, 2.3, 2.8$ and 2.9 TeV for $m_{\tilde{q}} \sim m_{\tilde{g}}$ and integrated luminosities of 10, 100, 1000 and 3000 fb^{-1} , respectively. For $\sqrt{s} = 14$ TeV, the LHC reach for the same integrated luminosities is to $m_{\tilde{g}} = 2.4, 3.1, 3.7$ and 4.0 TeV, respectively. The reach estimates for ab^{-1} luminosities may be over-optimistic due to low statistics of background with very hard cuts.

KEYWORDS: Supersymmetry Phenomenology, Supersymmetric Standard Model, Large Hadron Collider.

1. Introduction

The CERN Large Hadron Collider (LHC) is expected to begin collecting data from pp collisions at $\sqrt{s} \sim 10$ TeV, with a goal of accumulating $0.1 - 0.2 \text{ fb}^{-1}$ of usable data in the first run. During the very early stages of LHC running (first $\sim 0.1 \text{ fb}^{-1}$), detector commissioning will be in progress, and issues such as detector alignment and calibration will be addressed, as the experimental groups use familiar Standard Model (SM) processes such as $W + jets$, $Z + jets$ and $t\bar{t}$ production to guide the way. Running at 10 TeV is likely to continue for a year or more, after which it is expected that the center of mass energy will be increased, very likely in several stages, to its design value of 14 TeV.

While discovery of the Higgs boson (or bosons) or, more generally, the mechanism of electroweak symmetry breaking remains a primary goal of LHC experiments, an integrated luminosity of $\sim 10 \text{ fb}^{-1}$ will be required to claim Higgs discovery (if indeed $m_{\text{Higgs}} \sim 115 - 130$ GeV, as indicated by global analyses of electroweak data sets) [1]. An equally important objective for LHC is to discover, or exclude, weak scale supersymmetric (SUSY) matter. Since production cross sections for strongly interacting particles can range up to $\mathcal{O}(10^5)$ fb if $m_{\tilde{q}} \sim m_{\tilde{g}} \sim 400$ GeV at $\sqrt{s} = 10$ TeV, the hunt for supersymmetric particles beyond the reach of LEP2 and Tevatron searches could be very interesting even in the earliest stages of LHC running.

The discovery capability of LHC for SUSY particles is often illustrated with a reach plot in the parameter space of some assumed SUSY model [2]. At each point in SUSY model parameter space, many simulated collider events are generated, and compared against SM backgrounds with the same experimental signature[3]. Judicious cuts are then implemented to select out the new physics signals over SM backgrounds, and the signal is deemed observable if it satisfies pre-selected criteria for observability. The LHC reach has most frequently been analyzed [4] within the paradigm minimal supergravity (mSUGRA) model [5], but other SUSY models have also been studied.¹

In many models, production of strongly interacting SUSY particles is expected to yield the dominant signal channel, at least for $m_{\tilde{g}} \simeq m_{\tilde{q}} \lesssim 1.7$ TeV. Heavy squarks and gluinos then decay via complex cascades[11] which, if R -parity conservation is assumed, ends in the stable (or quasi-stable) lightest SUSY particle (LSP), often assumed to be the lightest neutralino \tilde{Z}_1 . The \tilde{Z}_1 escapes experimental detection, so that the generic SUSY signal is expected to be the production of multiple high E_T jets, multiple high p_T isolated leptons (e or μ , produced via the decays of chargino and neutralino secondaries) and possibly also isolated photons, together with missing transverse energy E_T^{miss} . The multiplicity of isolated leptons provides a convenient way to classify various SUSY signals [12], and for the mSUGRA model, reach contours have been shown for signals in the following channels:

- $jets + E_T^{\text{miss}}$ (no isolated leptons),

¹The LHC reach in anomaly-mediated SUSY breaking (AMSB) models is given in Ref. [6], in the mixed-modulus-anomaly mediation case in Ref. [7], while reach for various model lines in gauge mediated SUSY breaking (GMSB) is presented in Ref. [8], and for gaugino-mediated SUSY breaking in Ref. [9]. The LHC reach in mSUGRA with R -parity violation is presented in Ref. [10].

- $1\ell + jets + E_T^{\text{miss}}$,
- two opposite-sign isolated leptons (OS)+ $jets + E_T^{\text{miss}}$,
- two same-sign isolated leptons (SS)+ $jets + E_T^{\text{miss}}$,
- $3\ell + jets + E_T^{\text{miss}}$,
- $4\ell + jets + E_T^{\text{miss}}$,
- a real $Z \rightarrow \ell^+\ell^- + jets + E_T^{\text{miss}}$,
- a hard, isolated $\gamma + jets + E_T^{\text{miss}}$.

These explorations have typically been performed for the design LHC center-of-mass energy of $\sqrt{s} = 14$ TeV, and integrated luminosities of 10 or 100 fb^{-1} , anticipated after a year to a few years of running at the design luminosity.

Recently, some attention has been given to the ability of LHC to detect supersymmetric matter in the very earliest stages of running when a reliable measurement of E_T^{miss} , which requires a lead-time for detector alignment, calibration and understanding of the performance of essentially all detector components, will not be available [13]. In Ref. [14] it was instead suggested that in lieu of E_T^{miss} , high isolated lepton multiplicity could be used as a strong cut to reject SM backgrounds at relatively low cost to the expected SUSY signal: thus, requiring events with ≥ 4 jets plus OS, or SS, or three isolated leptons could allow for probes of $m_{\tilde{g}} \sim 500 - 600$ GeV with just 0.1-0.2 fb^{-1} of integrated luminosity. In a follow-up [15] paper, the authors refined and restricted their multi-lepton analysis to just multi-muons (because reliable electron identification may be difficult in the early stages of LHC running). The LHC reach was evaluated for $\sqrt{s} = 10$ TeV, and was found to be $m_{\tilde{g}} \sim 550$ GeV for 0.2 fb^{-1} in the SS dimuon plus ≥ 4 jets channel.² Alternatively, a search for acollinear dijet events was suggested by Randall and Tucker-Smith (RT-S)[16] as a SUSY search strategy that did not explicitly require E_T^{miss} . By cutting hard on several variables, a signal detectable over SM background was found, especially over portions of mSUGRA parameter space where squark pair production is significant and where the squarks decay directly into $q\tilde{Z}_1$.

In this paper, where we re-assess the LHC SUSY reach within the mSUGRA model, we have several goals:

1. We perform much more detailed SM background calculations than many previous works, including many $2 \rightarrow n$ subprocesses. In processes such as W , Z and $t\bar{t}$ production, we include exact parton emission matrix elements for the first several quark or gluon radiations (see details below). These calculations should model the multiple high E_T jet production in association with standard processes to much better accuracy than the parton shower method. In addition, we include numerous other subprocesses such as $Zt\bar{t}$ and $t\bar{t}b\bar{b}$ production, which have frequently been neglected.

²Indeed, muons are already being seen by ATLAS and CMS in cosmic ray events, and further, muons can be readily identified at lower p_T values than electrons, thus partially compensating for the loss of electron channel due to the increased muon signal efficiency.

	10 fb ⁻¹	100 fb ⁻¹	1000 fb ⁻¹	3000 fb ⁻¹
$\sqrt{s} = 10$ TeV	1.9 TeV	2.3 TeV	2.8 TeV	2.9 TeV (oFIT)
$\sqrt{s} = 14$ TeV	2.4 TeV	3.1 TeV	3.7 TeV	4.0 TeV (oFIT)

Table 1: Reach for the gluino mass for integrated luminosity values of 10, 100, 1000 and 3000 fb⁻¹ at $\sqrt{s} = 10$ TeV and 14 TeV, assuming $m_{\tilde{q}} \sim m_{\tilde{g}}$. The numbers for 1000 fb⁻¹ and 3000 fb⁻¹ should really be regarded as upper limits on the SLHC reach. For more details see Sec. 4.

2. We evaluate the LHC early discovery reach without E_T^{miss} cuts in two additional multi-muon channels – OS dimuons and trimuons – that have not yet been presented. We also show various distributions associated with these quantities that should lead to increased confidence that any observed excess arises from a real signal. We also evaluate the mSUGRA reach in the RT-S dijet channel, and compare with the multi-muon reach.
3. We present reach plots for the initial energy option of $\sqrt{s} = 10$ TeV, and compare with similar reach plots for $\sqrt{s} = 14$ TeV. We are motivated to do so because just how and when the center-of-mass energy of the LHC will be increased to its design value is presently unclear: if running full current through the superconducting magnets is deemed dangerous, or if it is deemed impractical to re-train the magnets that have “lost training” so that these cannot attain the full field, then it may be the case that LHC runs below the design energy for the first several years.
4. We show the LHC SUSY reach for a wide range of integrated luminosities, ranging from 0.05 fb⁻¹ (with cuts pertinent to early reach) up to 3000 fb⁻¹ with cuts optimized for the extraction of the SUSY signal. These high luminosity values would only be accessible at the SLHC, which is intended to upgrade the LHC luminosity to $\mathcal{L} = 10^{35}$ cm⁻²s⁻¹. We stress that several experimental challenges at such high luminosities would have to be overcome and our background MC might not be considered realistic for such luminosities.³ Our results for 1000 fb⁻¹ and 3000 fb⁻¹ are intended to provide an outer limit of the SLHC reach for its first few years of running. With this in mind, we show a summary of the LHC/SLHC reach for integrated luminosity values of 10, 100, 1000 and 3000 fb⁻¹ in Table 1.

The remainder of this paper is organized as follows. In Sec. 2, we present details of our improved SM background calculations, along with plots for the total background levels at $\sqrt{s} = 10$ and 14 TeV from various SM processes. In Sec. 3, we present *early* SUSY discovery reach plots in the various multimMuon channels, but with no E_T^{miss} cut, for several integrated luminosity values and $\sqrt{s} = 10$ TeV. We show several distributions that would serve to both distinguish the signal from SM backgrounds as well as to make a case for its SUSY origin. We also evaluate the LHC SUSY reach in the RT-S dijet channel. In Sec. 4, we show updated LHC reach plots for standard mSUGRA signal channels including E_T^{miss} cuts and our improved backgrounds, for $\sqrt{s} = 10$ and 14 TeV,

³For instance, multiple scattering effects will have to be accounted for.

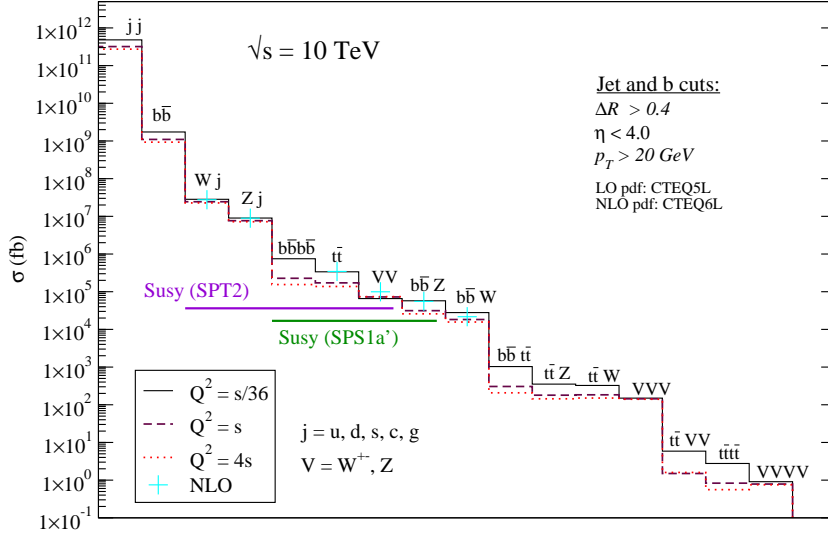


Figure 1: Total cross-sections for several SM backgrounds for pp collisions at $\sqrt{s} = 10$ TeV, with three different choices of renormalization and factorization scales (Q) (taken to be equal) shown by the solid ($Q = \sqrt{s}/6$), dashed ($Q = \sqrt{s}$) and dotted ($Q = 2\sqrt{s}$) lines. The NLO results are shown as blue crosses. The total cross-section for the SUSY SPS1a' and SPT2 mSUGRA cases are also shown for comparison purposes.

and a wide range of integrated luminosities. Because b -jet tagging, which can potentially increase the gluino reach by up to 20% in the mixed bino-higgsino LSP case that occurs in the so-called hyperbolic branch/focus point (HB/FP) region of the mSUGRA model [17], will be inefficient at the early stage and is presently uncertain in the ultra-high luminosity environment of the SLHC, we do not include it in the present analysis. Our ultimate plots include scans over a vast grid of possible cut values, so signal/background is optimized in various regions of model parameter space. We end with a summary of our results in Sec. 5.

2. Standard model background calculations

In order to understand how SUSY searches are affected by changes in the beam energy in the distinct channels, a careful assessment of the SM backgrounds is necessary. In particular, relaxing the E_T^{miss} cut may increase the contributions from different background processes that are usually neglected in the literature. We used AlpGen[18] and MadGraph[19] to compute the following $2 \rightarrow n$ processes: jj , $b\bar{b}$, $W^\pm j$, $Z^{(*)}j$, $\gamma^{(*)}j$, $b\bar{b}b\bar{b}$, $t\bar{t}$, VV , $b\bar{b}Z$, $b\bar{b}W^\pm$, $b\bar{b}t\bar{t}$, $t\bar{t}Z$, $t\bar{t}W^\pm$, VVV , $t\bar{t}VV$, $t\bar{t}t\bar{t}$ and $VVVV$, where j stands for light partons (u , d , s , c and g) and $V = W^\pm, Z$. The leading order (LO) total cross-sections for these processes at 10 TeV and 14 TeV are shown in Fig. 1 and 2. It is well known that at LO some of these cross-sections strongly depend on the choice of the renormalization (μ_R) and factorization (μ_F) scales (here we always take $\mu_F = \mu_R \equiv Q$). To estimate the systematic error from the scale dependence of the cross sections, we calculated these for three different scale choices: $Q = 2\sqrt{s}$, \sqrt{s} and $\sqrt{s}/6$. As expected, the processes which exhibit a strong dependence on the scale are the ones with $\sigma \propto \alpha_s^n$ ($n \geq 2$), as seen in Fig. 1 and 2. In particular, $\sigma(b\bar{b})$,

mass (GeV)	SPS1a'	SPT2
\tilde{g}	608	453
\tilde{q}	555	585
\tilde{t}_1	356	397
$\tilde{\mu}_L$	191	466
$\tilde{\mu}_R$	123	455
$\tilde{\nu}_\mu$	171	458
$\tilde{\tau}_1$	109	348
$m_{\tilde{\nu}_\tau}$	169	412
$m_{\tilde{W}_1}$	183	114
$m_{\tilde{Z}_1}$	98	64

Table 2: Representative sparticle masses for the two mSUGRA case study points labeled SPS1a' and SPT2 introduced in the text.

$\sigma(t\bar{t})$ and $\sigma(b\bar{b}b\bar{b})$ vary by factors of 1.8, 2.4 and 4.6, respectively. This scale dependence is basically the same at 10 and 14 TeV, with a small decrease ($\approx 10\%$) for the latter. Using MCFM[22] we computed the NLO total cross-sections for $t\bar{t}$, Wj , Zj , VV , $b\bar{b}W$ and $b\bar{b}Z$, with $Q = m_t$ for $t\bar{t}$ production, and $Q^2 = m_V^2 + p_T^2(V)$ for the the processes. The results are shown in Fig. 1 and 2. For the dominant backgrounds, namely Wj , Zj and $t\bar{t}$, the NLO results are well approximated by the LO cross-sections with the scale choice $Q = \sqrt{\hat{s}}/6$. Hence we choose this scale for all our subsequent background calculations. We point out that although our scale choice brings the total LO cross-section closer to the NLO result, the same is not necessarily true for the different kinematic distributions used in our analysis. However, to be conservative, we do not include a K factor for the signal cross-sections. We also show for comparison the total LO sparticle pair production cross sections for two mSUGRA points used here as case studies:

- SPS1a': $(m_0, m_{1/2}, A_0, \tan \beta, \text{sign}(\mu)) = (70 \text{ GeV}, 250 \text{ GeV}, -300 \text{ GeV}, 10, +)$,
- SPT2: $(m_0, m_{1/2}, A_0, \tan \beta, \text{sign}(\mu)) = (450 \text{ GeV}, 170 \text{ GeV}, 0 \text{ GeV}, 45, +)$

The SPS1a' [20] is a commonly adopted mSUGRA bench-mark point, while the second point (labeled SPT2 from here on) has a lighter gluino and slightly heavier squarks than SPS1a'.⁴ Representative sparticle masses for these cases are shown in Table 2.

Though squark and gluino masses are not hugely disparate for the two points, some aspects of the phenomenology are quite different. In the SPS1a' case, gluinos decay to squarks (with decays to tops and stops occurring about 20% of the time), and $\tilde{q}_L \rightarrow q'\tilde{W}_1$ decays occurring with a canonical branching fraction close to 2/3, and $BR(\tilde{q}_R \rightarrow q'\tilde{Z}_1) \simeq 1$. For the SPT2 case, squarks mainly decay to gluinos though $BR(\tilde{q}_L \rightarrow q'\tilde{W}_{1,2}) \simeq 0.3$, while gluinos decay via three body modes. The decay patterns of charginos and

⁴The point SPS1a' has been selected to yield the correct relic density of neutralino dark matter. The point SPT2 has much higher neutralino relic density, but is allowed in scenarios where there exists an axion/axino supermultiplet, in which case the DM consists of an axion/axino admixture[21] rather than neutralinos.

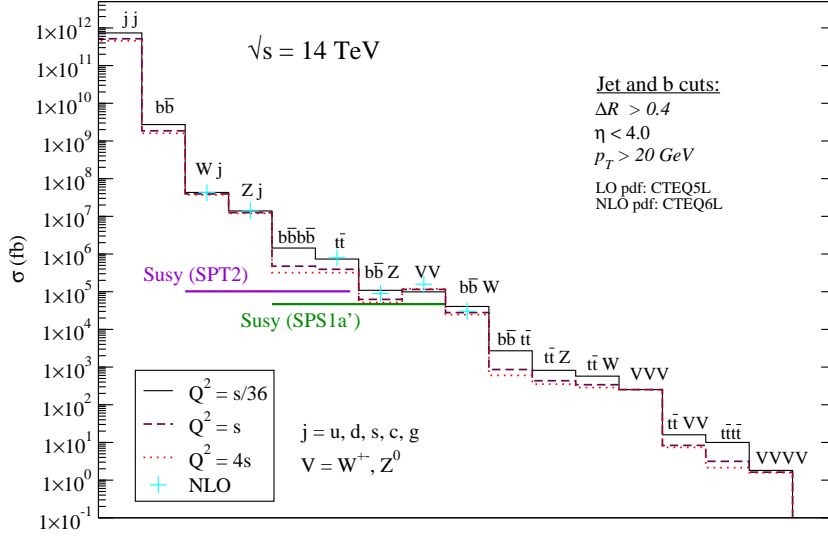


Figure 2: Total cross-sections for several SM backgrounds for pp collisions at $\sqrt{s} = 14$ TeV, with three different choices of renormalization and factorization scales (Q) (taken to be equal) shown by the solid ($Q = \sqrt{\hat{s}}/6$), dashed ($Q = \sqrt{\hat{s}}$) and dotted ($Q = 2\sqrt{\hat{s}}$) lines. The NLO results are shown as blue crosses. The total cross-section for the SUSY SPS1a' and SPT2 mSUGRA cases are also shown for comparison purposes.

neutralinos, however, differ in an important way between the two cases because for the SPS1a' case, $\tilde{\tau}_1$, \tilde{e}_R and $\tilde{\mu}_R$ are significantly lighter than \tilde{W}_1 and \tilde{Z}_2 , while the sneutrinos are just ~ 10 GeV lighter than \tilde{W}_1 and \tilde{Z}_2 . As a result, chargino and neutralino decays to stau – remember that the right sleptons, being singlets, have no coupling to winos – are significantly enhanced, resulting in a softer spectrum of muons (which frequently result as secondaries from τ decays) in the SPS1a' case. We will see below that this altered cascade decay pattern has a significant impact on the early detection of SUSY at the LHC: although squark and gluino masses are qualitatively similar, the SPT2 point is accessible at very low integrated luminosities, while detection in the SPS1a' case requires considerably larger integrated luminosity.

After verifying that for SUSY searches the most relevant backgrounds are $t\bar{t}$, Zj , Wj , jj , $t\bar{t}Z$ and $b\bar{b}Z$, we improved our results by adding multiple jets to these processes. Using AlpGen and the MLM matching algorithm[18] (to avoid double counting) we included in our background simulations the following processes: 2, 3, 4 jets, $t\bar{t}+0, 1, 2$ jets, $Z+0, 1, 2, 3$ jets, $W+0, 1, 2, 3, 4$ jets, $t\bar{t}Z+0, 1, 2$ jets, $b\bar{b}Z+0, 1, 2$ jets. In these processes $Z^{(*)}(\gamma^*) \rightarrow l\bar{l}, \nu\bar{\nu}$ ($l\bar{l}$) and $W^{(*)} \rightarrow l\nu$. Since we apply multijet and hard jet p_T cuts in our analysis (see below) the inclusion of the full matrix element results for the above processes significantly increases our background contributions to some of the search channels.

2.1 Event Simulation

For the simulation of the background events we use AlpGen and MadGraph to compute the hard scattering events and Pythia[23] for the subsequent showering and hadronization. The signal events were generated using Isajet 7.78[24]. A toy detector simulation is then

	All dimuons (fb)	$OS(\mu)$ (fb)	$SS(\mu)$ (fb)
$t\bar{t} + jets$ (Lres)	60.7 ± 5.7	47.3 ± 5.4	5.1 ± 1.1
$Z + jets$ (Lres)	80.6 ± 7.4	17.5 ± 3.4	0.0
Total BG (Lres)	141.3 ± 9.3	64.8 ± 6.4	5.1 ± 1.1
Signal (Lres)	60.1 ± 0.6	39.5 ± 0.5	12.0 ± 0.3
$t\bar{t} + jets$ (Dres)	61.6 ± 6.0	44.6 ± 5.3	3.7 ± 0.9
$Z + jets$ (Dres)	66.5 ± 6.7	15.4 ± 3.2	0.0
Total BG (Dres)	128.0 ± 9.0	60.0 ± 6.2	3.7 ± 0.9
Signal (Dres)	62.7 ± 0.8	41.0 ± 0.7	12.2 ± 0.4

Table 3: Comparison between different calorimeter resolutions for the ≥ 4 jets plus all, OS (with a veto for $m(\mu^+\mu^-) \leq 10$ GeV, and $75 \text{ GeV} < m(\mu^+\mu^-) < 105$ GeV) and SS dimuon channels for the dominant SM background ($Z + jets$ and $t\bar{t} + jets$) and the SUSY SPS1a' point. The statistical (MC) errors are also shown.

employed with calorimeter cell size $\Delta\eta \times \Delta\phi = 0.05 \times 0.05$ and $-5 < \eta < 5$. The HCAL (hadronic calorimetry) energy resolution is taken to be $80\%/\sqrt{E} + 3\%$ for $|\eta| < 2.6$ and FCAL (forward calorimetry) is $100\%/\sqrt{E} + 5\%$ for $|\eta| > 2.6$, where the two terms are combined in quadrature. The ECAL (electromagnetic calorimetry) energy resolution is assumed to be $3\%/\sqrt{E} + 0.5\%$. We use the Isajet[24] jet finding algorithm (cone type) to group the hadronic final states into jets. The jets and isolated lepton definitions are as follow:

- Jets are required to have $R \equiv \sqrt{\Delta\eta^2 + \Delta\phi^2} \leq 0.4$ and $E_T(jet) > 25$ GeV.
- Leptons are considered isolated if they have $p_T(l) > 5$ GeV with visible activity within a cone of $\Delta R < 0.2$ of $\Sigma E_T^{cells} < 5$ GeV.

2.2 Hadronic resolution and jet energy scale issues for early discovery

For our analysis of the early SUSY reach, we considered the possibility that the hadronic energy resolution may not be as good as anticipated, which could lead to an underestimate of those backgrounds such as $Z + jets$ that fall steeply with $E_T(j)$. Toward this end, we re-evaluated the most important backgrounds to dimuon production, assuming the hadronic energy resolution is only half as good as its default value above, *i.e.* we take,

- Low resolution (Lres): $160\%/\sqrt{E} + 3\%$ for $|\eta| < 2.6$ and $200\%/\sqrt{E} + 5\%$ for $|\eta| > 2.6$

instead of

- Default resolution (Dres): $80\%/\sqrt{E} + 3\%$ for $|\eta| < 2.6$ and $100\%/\sqrt{E} + 5\%$ for $|\eta| > 2.6$

The results are shown in Table 3.

We see that, with the worse resolution, the $Z \rightarrow \mu^+\mu^- + jets$ background cross section is indeed increased more than the corresponding cross section from the signal, or from the top background. However, after the invariant mass cut to veto Z 's the difference is

no longer striking. We conclude that hadronic calorimetry resolution is unlikely to be an issue, even for early detection of a signal.

One may also be concerned about background uncertainty from the jet energy scale. The $Z(\rightarrow \ell^+\ell^-) + j$ cross section is about 100 pb at the LHC, and can be used to establish the jet energy scale. The variation of the $Z + 4j$ cross section due to a 5% uncertainty in the jet energy scale is $\pm 20\%$ [25], which yields an estimate of the systematic uncertainty for SM background from this source. Since we will require the signal to background ratio to exceed 20% for observability (see Sec. 3), uncertainties in the background from the jet energy scale also appear to be under control.

3. Early SUSY discovery: searches at $\sqrt{s} = 10$ TeV with no E_T^{miss} cuts

After LHC turn-on in Fall 2009, a period of time will be used for detector studies and calibration. During this early phase, scheduled for about eleven months, the LHC will operate at $\sqrt{s} = 10$ TeV, and accumulate about 100-200 pb^{-1} of integrated luminosity [26, 25]. At this time, the classic SUSY signature of $jets + E_T^{\text{miss}}$ will almost certainly not be viable because of a number of issues related to measurement of missing transverse energy E_T^{miss} . While weakly interacting neutral particles such as neutrinos or the lightest neutralinos that escape detection in the experimental apparatus are the *physics* origin of E_T^{miss} , in practice missing transverse energy also arises from a variety of other sources, including:

- energy loss from cracks and un-instrumented regions of the detector,
- energy loss from dead cells,
- hot cells in the calorimeter that report an energy deposition even if there isn't one,
- mis-measurement in the electromagnetic calorimeters, hadronic calorimeters or muon detectors and
- mis-identified cosmic rays in events.

Thus, in order to have a solid grasp of expected E_T^{miss} from SM background processes, it will be necessary to have detailed knowledge of the *complete detector performance*. Experience at the Tevatron suggests that this complicated task may well take some time to complete at the LHC because many SM processes will have to be scrutinized in order to properly calibrate the detector. For this reason, SUSY searches using the classic $jets + E_T^{\text{miss}}$ signature, or for that matter *any* signature with E_T^{miss} as a crucial requirement, may well take longer than a year to yield reliable results.

On the other hand, if sparticles are relatively light – not far beyond the reach of Tevatron searches [29] – then their production cross sections at the LHC can be huge, and tens of thousands of new physics events may be produced in the first few months of LHC operation. For instance, for $m_{\tilde{g}} \sim 400$ GeV and heavy squarks, the expected gluino pair cross sections are in the 10^4 fb range. If $m_{\tilde{g}} \sim m_{\tilde{q}} \sim 400$ GeV, then SUSY production cross

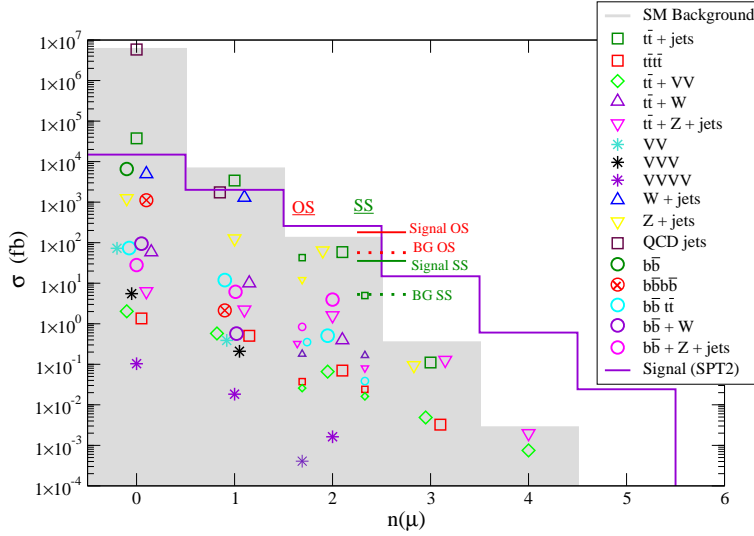


Figure 3: Cross sections for various multiplicities of isolated muons in n -muon $+ \geq 4$ jet events at the LHC, with $\sqrt{s} = 10$ TeV. We show the signal levels for the SPT2 sample point by the open histogram, along with corresponding levels for various SM backgrounds. In the $n(\mu) = 2$ bin, the left, center and right columns show the background components for SS, dimuons and OS (with invariant mass cuts), respectively.

sections are even higher: of order 10^5 fb! Thus, with just 0.1 fb^{-1} of integrated luminosity, we might expect of order $10^3 - 10^4$ new physics events to be recorded on tape if the gluino is in the 400 GeV range. These large rates provide motivation to re-evaluate search strategies that may be reliably carried out at the earliest stages of LHC operation at $\sqrt{s} = 10$ TeV. To avoid a complicated analysis of the rate at which jets fake electrons which will be rather uncertain during early running, we focus on signals involving only muons and jets, and where precise determination of the energies does not play a crucial role in the extraction of the signal over background. Identification of high p_T muons, on the other hand, is one of the most straightforward measurements at LHC, and the ATLAS and CMS detectors are utilizing cosmic ray muons as a tool for understanding their detectors even before the LHC turn-on.

In what follows, we define the signal to be observable if

- $S \geq \max[5\sqrt{B}, 5, 0.2B]$

where S and B are the expected number of signal and background events, respectively. The requirement $S \geq 0.2B$ is imposed to avoid the possibility that a *small* signal on top of a *large* background could otherwise be regarded as statistically significant, but whose viability would require the background level to be known with exquisite precision in order to establish a discovery.

3.1 LHC reach in multi-muon + jets channels without E_T^{miss} requirements

The center-of-mass energy of 10 TeV is a five-fold increase on the highest collision energies currently attained and, as just discussed, represents an opportunity for sparticle searches

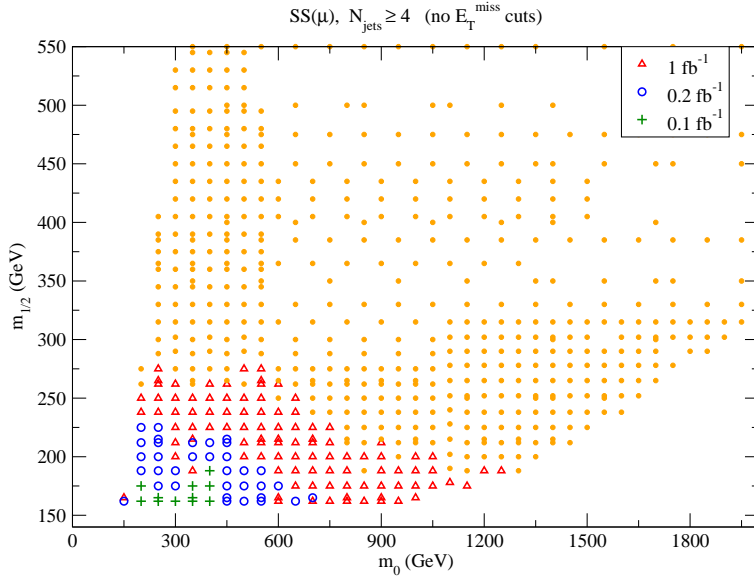


Figure 4: SUSY reach of the LHC at $\sqrt{s} = 10$ TeV via SS-dimuon plus ≥ 4 jets events with only the basic cuts detailed in the text, for various integrated luminosities. The fixed mSUGRA parameters are $A_0 = 0$, $\tan\beta = 45$ and $\mu > 0$. The solid dots here, and in other subsequent figures, denote model points where the signal remains unobservable even for the largest integrated luminosity shown in the figure.

well beyond the reach of the Fermilab Tevatron. Motivated by this, we follow up on earlier studies [14, 15] and explore the early reach of the LHC in the relatively straightforward multi-muon plus multi-jet channels where precise energy measurements are not essential, and complications due to jets faking an electron are absent. We impose the following basic cuts⁵

- Jet cuts: $n(jets) \geq 4$ with $E_T(j_1) \geq 100$ GeV, $E_T(j) \geq 50$ GeV and $|\eta(j)| \leq 3.0$ (jets are ordered $j_1 - j_n$, from highest to lowest E_T)
- $S_T \geq 0.2$, where S_T is the transverse sphericity,
- Muon cuts: $p_T(\mu) \geq 10$ GeV, $|\eta(\mu)| \leq 2.0$, $10 \text{ GeV} \leq m(\mu^+\mu^-) \leq 75$ GeV or $m(\mu^+\mu^-) \geq 105$ GeV (for OS muons only),

and plot in Fig. 3 the surviving cross section versus the muon multiplicity for the SUSY SPT2 point, along with corresponding contributions from a variety of $2 \rightarrow n$ SM background processes at $\sqrt{s} = 10$ TeV. At low muon multiplicity, signal is well below the background, which is dominated by QCD multi-jet production for $n_\mu = 0$, and by $t\bar{t}$, $W + j$ and QCD production for $n_\mu = 1$. For $n_\mu = 2$, we see that the signal and background are already comparable. We can further divide the dimuon events into the OS and SS class. For OS dimuons we apply the invariant mass cuts listed above to avoid the γ^* , $Z \rightarrow \mu^+\mu^-$ poles. In this case, the signal (for this sample point) is seen to exceed the background in

⁵Unless stated otherwise, these cuts are imposed on all muon plots in what follows.

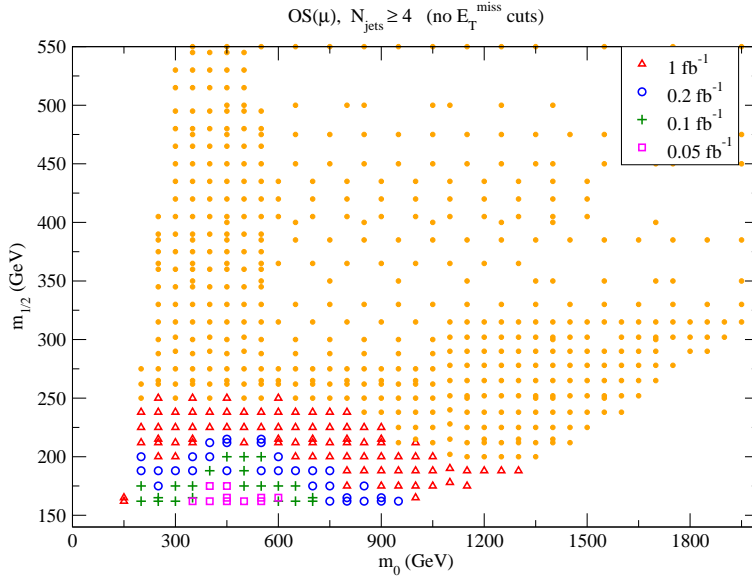


Figure 5: SUSY reach of the LHC at $\sqrt{s} = 10$ TeV via OS-dimuon plus ≥ 4 jets events with only the basic cuts detailed in the text, for various integrated luminosities. The fixed mSUGRA parameters are $A_0 = 0$, $\tan\beta = 45$ and $\mu > 0$.

both the OS and SS channels. We also mention that the SS dimuon cross section from $W^\pm W^\pm + dd/uu$ production is negligible: specifically, $\sigma(pp \rightarrow W^+W^+ + X) = 116$ fb, $\sigma(pp \rightarrow W^-W^- + X) = 46$ fb, and this contribution to the $\mu^+\mu^+ + 4j$ ($\mu^-\mu^- + 4j$) cross section in Fig. 3 is just 0.015 fb (0.008 fb). Moving to the 3μ channel, we see that the signal drops, but the background, which is dominated by Z , $t\bar{t}$ and $t\bar{t}Z$ production, drops even further. The $3\mu + \geq 4$ jets signal is at the 15 fb level, while the corresponding background is around 0.34 fb: despite the fact that the statistical significance as well as the $S : B$ ratio are both largest for the trimuon case, an integrated luminosity in excess of 300 pb^{-1} is necessary to attain the five-event level that we require for observability.

In Fig. 4, we show the reach of the $\sqrt{s} = 10$ TeV LHC for the clean SS dimuon plus ≥ 4 jets events for various values of integrated luminosity, using only the basic jet, S_T and muon cuts mentioned above. We scan over the mSUGRA model parameters m_0 and $m_{1/2}$, with $A_0 = 0$, $\tan\beta = 45$ and $\mu > 0$. We see that with just 0.1 fb^{-1} , already values of $m_{\tilde{g}} \sim 450$ GeV become accessible. As the integrated luminosity is increased to 0.2 (1) fb^{-1} , the reach increases to 550 (650) GeV.

In Fig. 5, we plot the corresponding reach of the $\sqrt{s} = 10$ TeV LHC for OS dimuon plus ≥ 4 jets events for various values of integrated luminosity. For low values of $m_{1/2}$, this signature appears to be even more promising than the SS dimuon channel since this signal is observable over portions of the parameter space with $m_{\tilde{g}} \lesssim 450$ GeV with just 50 pb^{-1} of integrated luminosity!⁶ We see, however, that for larger integrated luminosities (for which the SS dimuon signal crosses the five-event level), the reach via the SS channel,

⁶We should temper this conclusion with some caution, since it is contingent upon our background estimate being correct. In practice, the SM background in the dimuon plus $\geq 4j$ channel will likely be extracted from the data. Assuming that $t\bar{t}$ events are the dominant source of this background, we estimate

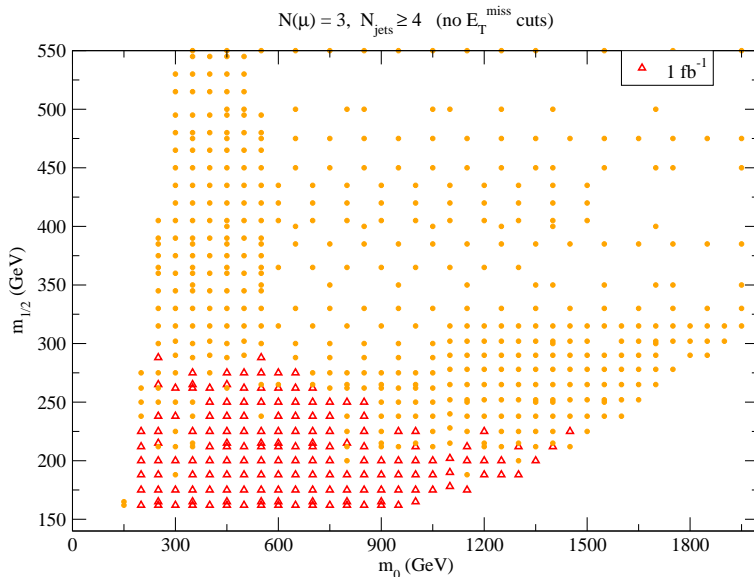


Figure 6: SUSY reach of the LHC at $\sqrt{s} = 10$ TeV via trimuon plus ≥ 4 jets events with only the basic cuts detailed in the text, for various integrated luminosities. The fixed mSUGRA parameters are $A_0 = 0$, $\tan\beta = 45$ and $\mu > 0$.

which has a larger $S : B$ ratio, exceeds that in the OS channel. In the OS dimuon channel, the reach in $m_{\tilde{g}}$ is 500 (600) GeV for an integrated luminosity of 0.2 (1) fb^{-1} . We should remember that the projections for especially 1 fb^{-1} are conservative, since it is likely that by the time this is accumulated, the detectors will be well enough understood for the E_T^{miss} as well as the electron channels to be useful.

In Fig. 6, we plot the reach of the $\sqrt{s} = 10$ TeV LHC for the trimuon plus ≥ 4 jets events for various values of integrated luminosity. Due to the smaller signal cross-section (compared to the dimuon channels), the trimuon signal remains below observability for even 200 pb^{-1} of integrated luminosity. However, due to the large signal to background ratio, even with just 1 fb^{-1} , this low-rate but relatively background-free channel probes gluino masses up to ~ 700 GeV.

3.2 Characteristics of SUSY multi-muon + jets events

While a discovery of an excess of SS, OS or 3μ plus jets events would be exciting, it would also be useful to check various aspects of these multi-muon events to see if they agree with a hypothetical origin from supersymmetry. This is especially crucial for any discussion of early SUSY discovery where the signal may initially comprise of just 5-10 events over a very small SM background. With this in mind, we study various muon (and some jet) distributions: any signal in the “counting experiments” of Sec. 3.1 will be that much more convincing if these events have the expected characteristics discussed below. As the accumulated integrated luminosity grows, these same distributions (with electrons

that an integrated luminosity of 20-30 pb^{-1} will suffice to extract this background from the measurement of the $t\bar{t}$ cross section with additional jets.

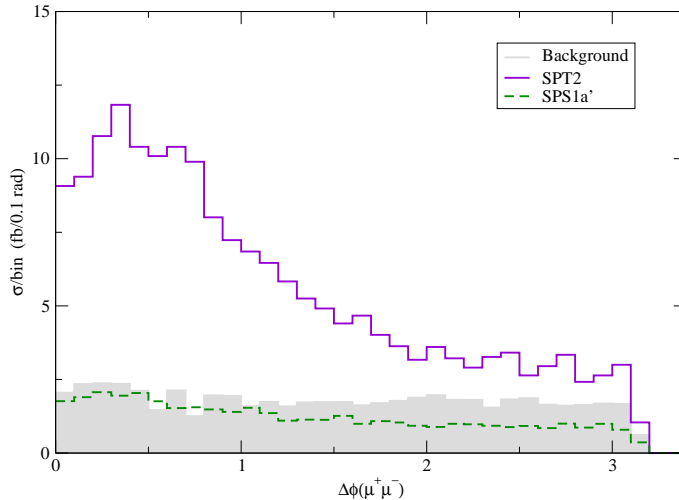


Figure 7: $\Delta\phi(\mu^+\mu^-)$ distribution from OS dimuon + ≥ 4 jets events for SPS1a' (dashed) and SPT2 (solid) cases, and also for SM backgrounds (shaded). We make no requirement on E_T^{miss} .

combined with muons) will, of course, provide more precise information about sparticle masses, which will help to zero in on the underlying model. We show these distributions for the two SUSY cases SPS1a' and SPT2 introduced above as well as for the SM background, beginning with OS dimuon channel which has the potential for the earliest discovery of SUSY.

3.2.1 Opposite sign dimuon + jets events

We begin by illustrating in Fig. 7 the distribution of the transverse plane opening angle $\Delta\phi(\mu^+\mu^-)$ between the muons on OS dimuon + ≥ 4 jets events from the SPS1a' (dashed), the SPT2 (solid) SUSY cases and from the SM background (shaded). We see that for the SPT2 point where a large fraction of the muons originate from high p_T $\tilde{Z}_2 \rightarrow \mu^+\mu^-\tilde{Z}_1$ produced in gluino and squark cascade decays; this distribution peaks at small angles. The distribution tail comes from dimuons originating from cascade-decay-produced charginos and extends out to $\Delta\phi(\mu^+\mu^-) \sim \pi$. For the SPS1a' point, the stau is light, and so a much smaller fraction of muons come from direct decays of \tilde{Z}_2 , and the corresponding distribution is much flatter. The difference between the two signal distributions is a reflection of the different origins of the muons in the two cases. The SM background is nearly flat, but also with a slight peak at low values of $\Delta\phi$.

The distribution of the invariant dimuon mass $m(\mu^+\mu^-)$ in OS dimuon + $\geq 4j$ events shown in Fig. 8 is even more distinctive. In this case, the SPT2 signal distribution shows the distinctive kinematic mass edge[27] at $m(\mu^+\mu^-) = m_{\tilde{Z}_2} - m_{\tilde{Z}_1} = 50.6$ GeV. In this case, most of the signal dimuons would be expected to cluster just below 50 GeV, strengthening the case for the SUSY origin of a signal in the earliest data set. For the SPS1a' case (which, we emphasize, is somewhat atypical), the mass edge from $\tilde{Z}_2 \rightarrow \tilde{\mu}^\pm\mu^\mp \rightarrow \mu^+\mu^-\tilde{Z}_1$ decays (which have a branching fraction of just 2.4%) at ~ 82 GeV is considerably less distinctive. Moreover, this edge merges right into the Z peak, and so will not be measurable.

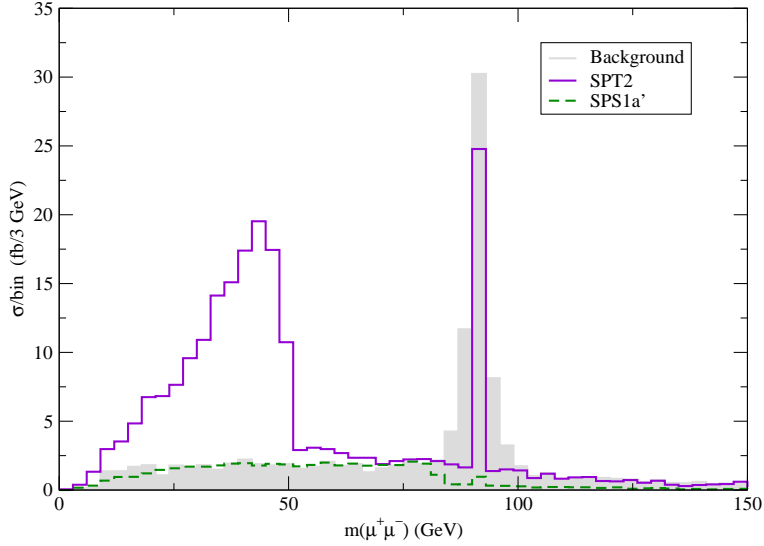


Figure 8: OS dimuon invariant mass distribution from OS dimuon + ≥ 4 jets events for SPS1a' (dashed) and SPT2 (solid) cases, and also for SM backgrounds (shaded). In this plot only we do not apply the invariant mass cuts for OS dimuons. We make no requirement on E_T^{miss} .

Furthermore, notice that this distribution is smeared out to low mass values because both \tilde{Z}_2 and \tilde{W}_1 decay dominantly to third generation sleptons, and the muon is frequently produced as a secondary from tau decays. Except for the Z -peak, the SM background is featureless.

Finally, in Fig. 9 we show the $\sum E_T(\text{jet})$ distribution for events with OS dimuons + ≥ 4 jets events: the large energy release occurring in sparticle pair production and decay provides a harder distribution than that expected from SM background. We see that in both cases it should be possible to pick out the signal over the background using only the measured transverse energies of the jets, though for the SPS1a' case, with the smaller cross section, a somewhat larger integrated luminosity will be required.

3.2.2 Same sign dimuon + jets events

As mentioned in Sec. 3.1, the SS dimuon channel requires larger integrated luminosity (due to its reduced rate), but provides a much cleaner signal. To get an idea of the overall $p_T(\mu)$ distribution in this channel, we show in Fig. 10 this distribution for the hard (μ_1) and soft (μ_2) muons from SS dimuon events without any jet cuts for the signal points SPS1a' and SPT2 and for the background, which mainly comes from $t\bar{t}$ production. While the highest p_T muon from $t\bar{t}$ production comes from $t \rightarrow bW$ followed by $W \rightarrow \mu\nu_\mu$ decay, and is quite hard, the lower p_T muon must come from $b \rightarrow c\mu\nu_\mu$ decay, and hence is necessarily soft, since there is much less energy release in b decays. Thus, while the signal emerges from the background only for $p_T(\mu_1) \gtrsim 100 - 125$ GeV, the soft muon from the signal – likely arising from some heavy sparticle decay – has a much harder distribution than the corresponding background muon. For this reason, we require $p_T(\mu_2) > 10$ GeV, even though it might be possible for LHC detectors to go even lower in muon transverse momentum. We see again that the SPS1a' case is not the norm in that especially the lower energy signal muon frequently arises from tau decay, and so is also soft.

Next, we show in Fig. 11 the distribution of the transverse plane opening angle between the two muons in SS events with ≥ 4 jets, again for both SPS1a' and SPT2 signals and for the SM background. This distribution differs sharply from the corresponding distribution for OS dimuon events shown in Fig. 7 in that the signal is peaked near $\Delta\phi \sim \pi$. This shape is merely a reflection of the fact that in the SS case the two muons typically originate from *different* primary particles in the SUSY $2 \rightarrow 2$ ($\tilde{g}\tilde{g}$, $\tilde{g}\tilde{q}$, or $\tilde{q}\tilde{q}$) production subprocess, in contrast to OS dimuons from neutralino decays. The background distribution is nearly flat in $\Delta\phi(\mu^\pm\mu^\pm)$.

We have checked that the shape of the distribution of $\sum E_T(j)$ in SS dimuons + $\geq 4j$ events is qualitatively similar to that for OS dimuon events shown in Fig. 9, and so we do

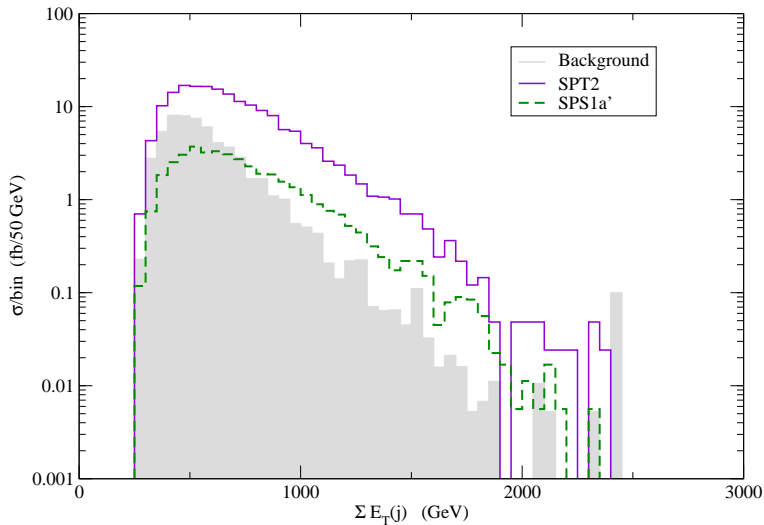


Figure 9: Distribution of $\sum E_T(j)$ for OS dimuon + ≥ 4 jets events from signal cases SPS1a' (dashed) and SPT2 (solid), and from SM backgrounds. We make no requirement on E_T^{miss} .

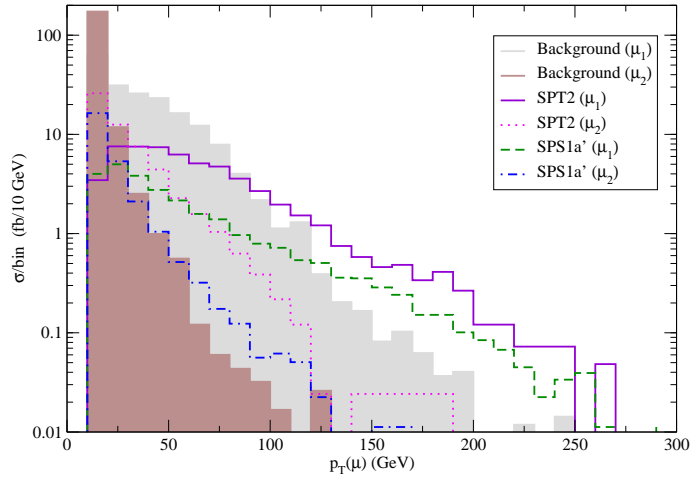


Figure 10: p_T distribution for the harder (μ_1) and softer (μ_2) muons in SS dimuon events for the SUSY SPS1a' and SPT2 mSUGRA cases, along with corresponding SM background distributions. We make no requirement on number of jets or E_T^{miss} .

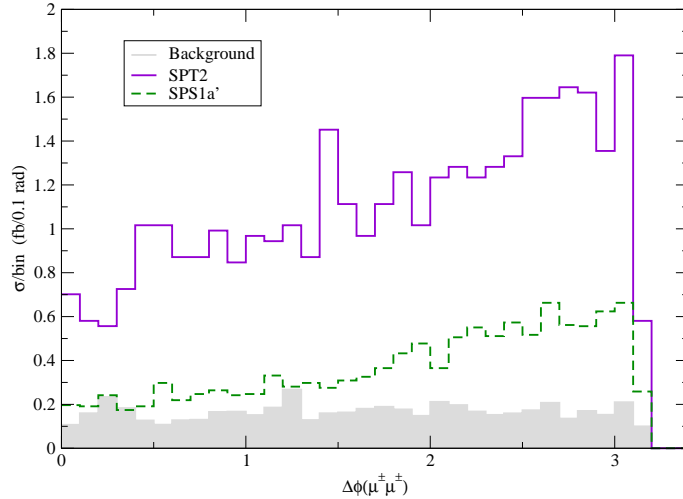


Figure 11: Distribution of the transverse plane opening angle between the muons, $\Delta\phi(\mu^\pm\mu^\pm)$, from SS dimuon + $\geq 4j$ events for the SUSY cases SPS1a' and SPT2, along with the corresponding distribution from SM sources. We make no restriction on E_T^{miss} .

not show it here.

3.2.3 Trimuon + jets events

Because it has an even smaller background, the trimuon channel – at a high enough integrated luminosity – could potentially become the best muon channel for SUSY searches without E_T^{miss} cuts. In Fig. 12a, we show the trimuon invariant mass distribution from $3\mu + \geq 4$ jets events for the SUSY points SPS1a' and SPT2, along with that from the SM background at $\sqrt{s} = 10$ TeV. As expected, the signal distribution is relatively featureless, since at least two of the muons originate in different parent particles. The trimuon cross

section is small – 14.8 fb for SPT2 point, and 3.2 fb for the SPS1a' case – so that even with 1 fb^{-1} only the former case leads to an observable signal in Fig. 6.

The noteworthy thing, however, is that though the signal is very small, it is almost background-free, even with just the basic cuts. Thus this channel offers prospects for a striking confirmation of new physics (presumably first discovered in the OS dimuon channel). In most SUSY models we expect that $m_{\tilde{W}_1}$ is comparable to $m_{\tilde{Z}_2}$, so that if \tilde{Z}_2 can be produced in gluino and squark cascade decays, the chargino can usually also be produced via these decay cascades. Thus a subsample of trimuon events is likely to include an OS muon pair from \tilde{Z}_2 decays. With this in mind, we show the distribution of the *smaller* of the two OS dimuon invariant masses in these tripleton $+ \geq 4j$ events in frame *b*) of this figure. For both cases, we see a mass edge at essentially the same location as in Fig. 8, and further, that below the mass edge, the two distributions are very similar, reflecting the common parentage of the dimuons in the two cases. In favorable cases such as SPT2, the trimuon signal could thus make a strong case for the SUSY origin of a signal first seen with just $\sim 50 - 200 \text{ pb}^{-1}$ of the LHC data. For the SPS1a' point, the trimuon signal offers the possibility of determining the mass edge (obscured by the Z peak in the OS dilepton case), though an integrated luminosity of $\sim 10 \text{ fb}^{-1}$ may be required (by which time it is likely that electron events will also be possible to include in the tripleton sample).⁷

Finally, we remark that the $\sum E_T(j)$ distribution for $3\mu + \geq 4$ jets events is again harder than that for the SM background; since its features are again much the same as in Fig. 9, we do not show it here.

3.2.4 Early LHC reach via multimuons plus jets: optimized cuts

We have seen from the various reach plots presented in Sec. 3.1 that even with very basic cuts, and just $0.1 - 1 \text{ fb}^{-1}$ of integrated luminosity, LHC experiments will probe gluino and squark masses well beyond the reach of the Tevatron. These cuts have not, however,

⁷Events beyond the mass edge arise, for instance, from $\tilde{g} \rightarrow t\bar{t}_1$ decays, as well as from Z s produced in \tilde{Z}_3 decays in the SPT2 case.

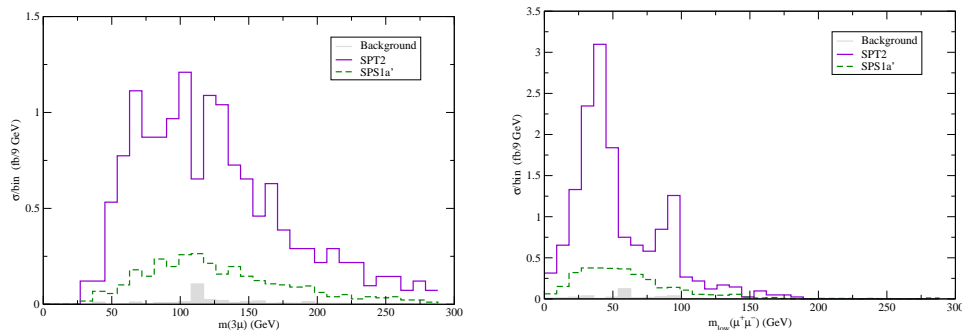


Figure 12: The distribution of (a) trimuon mass, and (b) the smaller of the two OS dimuon invariant masses, from trimuon $+ \geq 4$ jets events at the 10 TeV LHC for SUSY points SPS1a' and SPT2, along with SM backgrounds.

been optimized over different regions of parameter space, and so will not yield the maximal reach for a given value of integrated luminosity. In this section, we implement a large grid of potential cut values, and then select the grid (set of cuts) value which optimizes the reach. We recognize that this may be only of academic interest in that by the time such an analysis is actually carried out, LHC detectors may be understood well enough to allow the inclusion of electrons as well as E_T^{miss} in the analysis. We nevertheless felt that it would be worthwhile to explore just how much information can be gleaned from the data, in case circumstances make this necessary.

We begin with a set of pre-cuts:

- transverse sphericity $S_T \geq 0.2$,
- for isolated muons: $p_T(\mu) \geq 10$ GeV and $|\eta(\mu)| < 2.0$,
- $n(\text{jets}) \geq 2$ with $E_T(j) \geq 50$ GeV and $|\eta(j)| < 3.0$,
- for OS dimuons: $10 \text{ GeV} \leq m(\mu^+\mu^-) \leq 75 \text{ GeV}$ or $m(\mu^+\mu^-) > 105 \text{ GeV}$

Then, for a given point in mSUGRA parameter space with of order 50,000 events generated, we find the optimal set of cuts to maximize $S/\sqrt{B+S}$, using:

- $n(\text{jets}) \geq 2, 3, 4, 5, 6, 7$
- $E_T(j_1) \geq 50, 80 - 340$ GeV (in steps of 20 GeV), $400 - 1000$ GeV (in steps of 100 GeV),
- $E_T(j_2) \geq 50, 55 - 205$ GeV (in steps of 15 GeV), $300, 400, 500$ GeV,
- number of isolated muons $n(\mu) = 2, 3, 4, 5, 6$

We do not implement any E_T^{miss} requirement. We take $\sqrt{s} = 10$ TeV, and adopt standard parameters $A_0 = 0$, $\tan \beta = 45$ and $\mu > 0$. The results of our optimized cuts analysis is shown in Fig. 13 for various integrated luminosity choices. We note the following:

- for low integrated luminosities (0.05 fb^{-1} and 0.1 fb^{-1}) the optimal cuts are $n(\text{jets}) \geq 4, 5$ with $E_T(j_1) \sim 100$ GeV and $E_T(j_2) \sim 70$ GeV in the total dimuon channel.
- the same is also true for 0.2 fb^{-1} and 1 fb^{-1} , except for $m_0 \gtrsim 1200$ GeV and/or $m_{1/2} \gtrsim 320$ GeV, where the $n(\text{jets}) \geq 6, 7$ channels become more favorable. Moreover the preferred jet E_T cuts are always below 200 GeV for $0.05, 0.1$ and 0.2 fb^{-1} and below 300 GeV for 1 fb^{-1} .

We caution the reader that the projected reaches will be sensitive to the uncertainty in our estimate of the background, especially for high jet multiplicities. It is, however, worth bearing in mind that even after optimization, the bulk of the parameter space is probed with $n_j \geq 4, 5$ and $n_\mu = 2$.⁸ The optimized low m_0 reach from Fig. 13 extends up to $m_{1/2}$ values of 225, 275 and 325 GeV for integrated luminosity values of $0.1, 0.2$ and 1 fb^{-1}

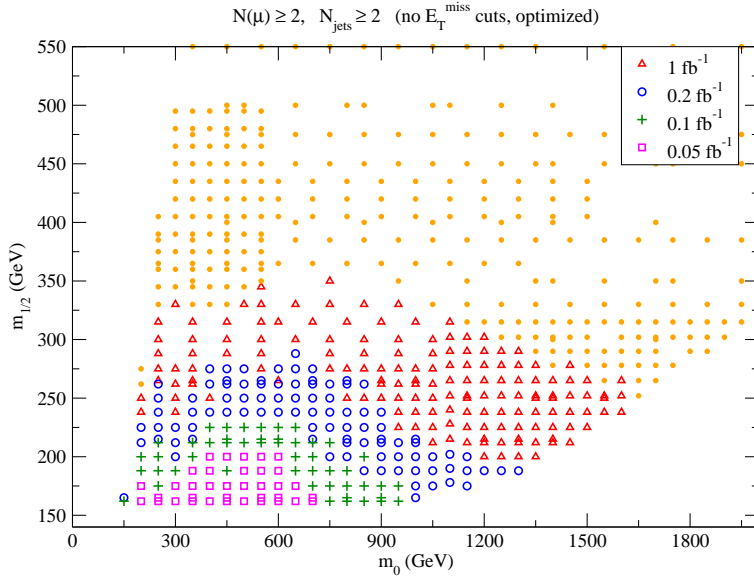


Figure 13: Reach of LHC for mSUGRA at $\sqrt{s} = 10$ TeV for multi-muon $+jets$ events using optimized cuts discussed in the text, but without any E_T^{miss} requirement on the signal. The fixed mSUGRA parameters are $A_0 = 0$, $\tan\beta = 45$ and $\mu > 0$.

respectively. This corresponds to a reach in terms of $m_{\tilde{g}}$ of about 600, 700 and 800 GeV, respectively.

With accumulation of integrated luminosity, the detectors will rapidly become better understood and reliable electron identification will be possible. It will then be possible to use different flavor, OS dilepton distributions to statistically subtract chargino and W contributions from the same flavor, OS dilepton signal and sharpen up the dilepton mass edge first obtained in Fig. 8. Using the same cuts (except that we now include electrons) as in Fig. 7 and 8, we plot the distribution of $\Delta\phi(e^\pm\mu^\mp)$ in Fig. 14, and the “subtracted” like-flavor, OS dilepton mass distribution,

$$\frac{d\sigma}{dm}(e^+e^- + \mu^+\mu^- - e^+\mu^- - e^-\mu^+) = \frac{d\sigma(e^+e^-)}{dm_{ee}} + \frac{d\sigma(\mu^+\mu^-)}{dm_{\mu\mu}} - \frac{d\sigma(e^+\mu^-)}{dm_{\mu e}} - \frac{d\sigma(e^-\mu^+)}{m_{e\mu}}, \quad (3.1)$$

in Fig. 15.

⁸This has the added advantage that even the “trials factor” is greatly reduced.

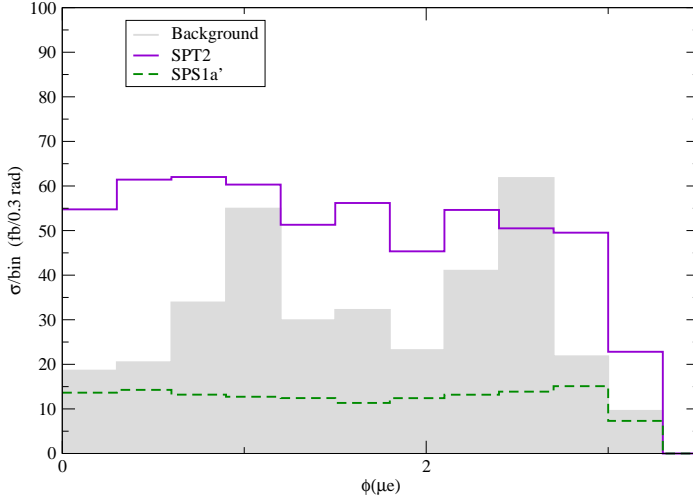


Figure 14: $\Delta\phi(e^\pm\mu^\mp)$ for the mSUGRA points SPS1a' and SPT2 at $\sqrt{s} = 10$, along with SM backgrounds. The lepton and jet cuts are as in Fig. 7, and there is no requirement on E_T^{miss} .

We see that the azimuthal angular distribution of $\Delta\phi(\mu^\pm e^\mp)$ is rather flat, as may be expected since the leptons arise from various decay chains including $\tilde{g} \rightarrow t\tilde{b}\tilde{W}_1$ (SPT2 case) and $\tilde{g} \rightarrow t\tilde{t}_1$ (SPS1a' case) which can give $e^\pm\mu^\mp$ pairs from the decay of the same gluino in addition to $e^\pm\mu^\mp$ pairs where the electron and muon each originate in a different gluino (or squark) parent (as in the SS dilepton case). As anticipated, the dilepton mass edges become significantly sharper upon flavor-subtraction, though the Z peak continues to obscure the edge in the SPS1a' case. Of course, this subtraction procedure ought to work equally well for the triplepton signal shown in Fig. 12b, with the understanding that the dilepton pairs in (3.1) now refer to the OS dilepton pair in triplepton events with the

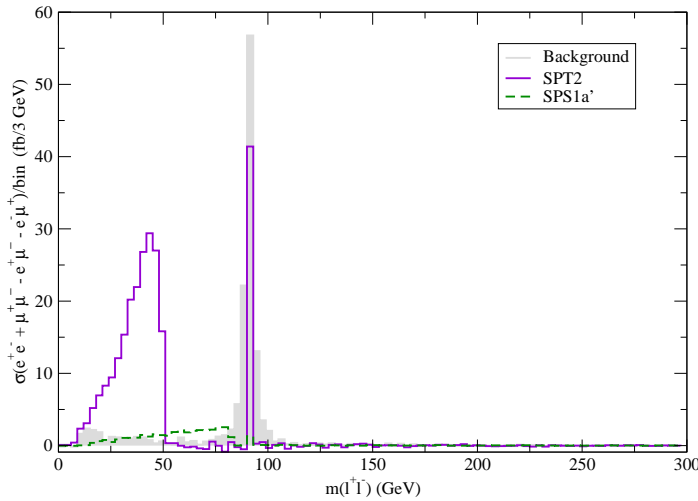


Figure 15: The subtracted like-flavor, OS dilepton mass distribution for the mSUGRA points SPS1a' and SPT2 at $\sqrt{s} = 10$, along with SM backgrounds. The lepton and jet cuts are the same as in Fig. 8, and there is no requirement on E_T^{miss} .

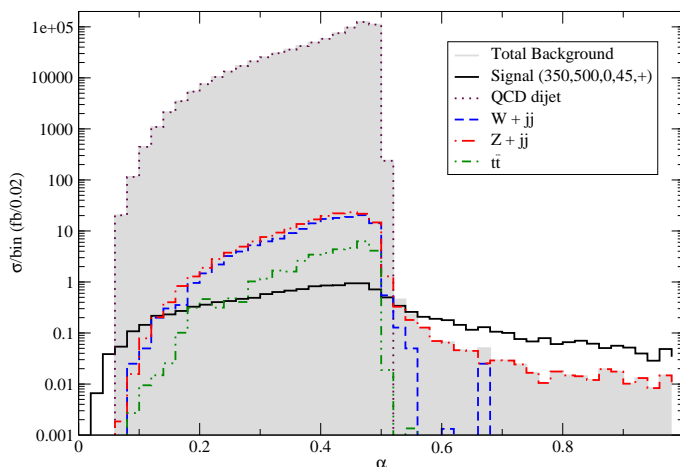


Figure 16: Distribution of $\alpha = E_T(j_2)/m(j_1 j_2)$ for dijet events with no identified leptons for the mSUGRA point $m_0 = 350$ GeV, $m_{1/2} = 500$ GeV, $A_0 = 0$ GeV, $\tan\beta = 45$ and $\mu > 0$ at $\sqrt{s} = 10$ TeV, along with corresponding distributions from various SM sources. The fixed mSUGRA parameters are $A_0 = 0$, $\tan\beta = 45$ and $\mu > 0$. We require that $E_T(j_1) + E_T(j_2) > 700$ GeV, but make no restriction on E_T^{miss} .

smaller of the two masses.

3.3 Early LHC reach in dijet channel at $\sqrt{s} = 10$ TeV

Recently, Randall and Tucker-Smith (RT-S)[16] have proposed a search for SUSY in the dijet channel, also without using E_T^{miss} . While SUSY dijet + E_T^{miss} searches have been proposed for a long time, RT-S emphasized that the search can be made without recourse to an E_T^{miss} cut. RT-S propose selecting events with exactly two jets with $E_T > 50$ GeV and no isolated leptons. This probes the small m_0 region of the mSUGRA space because $\tilde{q}_R \tilde{q}_R$ pair production naturally leads to this event topology, since for $m_{\tilde{q}} < m_{\tilde{g}}$, \tilde{q}_R mainly decays via $\tilde{q}_R \rightarrow q \tilde{Z}_1$. RT-S then examine distributions of a) $\alpha \equiv E_T(j_2)/m(j_1 j_2)$, b) $\Delta\phi(j_1 j_2)$ (the dijet transverse plane opening angle) and c) the variable $E_T(j_1) + E_T(j_2)$. Signal was found to exceed SM background for appropriate intervals of each of these variables, for mSUGRA points with light squarks, where the squark-squark and squark-gluino production cross-sections are enhanced.

Following RT-S, we evaluate signal and background for the LHC start-up energy of $\sqrt{s} = 10$ TeV, and plot the α and $\Delta\phi$ distributions for the mSUGRA point $m_0 = 350$ GeV, $m_{1/2} = 500$ GeV, $A_0 = 0$ GeV, $\tan\beta = 45$ and $\mu > 0$. This mSUGRA point has moderately heavy gluinos and squarks ($m_{\tilde{g}} = 1160$ GeV, $m_{\tilde{q}} \sim 1000$ GeV) and is *not accessible* via early searches in the multimueon channels. After imposing a $E_T(j_1) + E_T(j_2) > 700$ GeV cut for both signal and background we see from Figs. 16 and 17 that for appropriate cuts on α and $\Delta\phi$ to remove the enormous QCD background, the signal is above the remaining background, which mainly comes from the $Z + 2j$ production, where the Z decays invisibly. Dijet events with the required geometry from Wjj and $t\bar{t}$ production arise only if one (or more) of the visible decay products of W or t is missed in the detector. We mention here

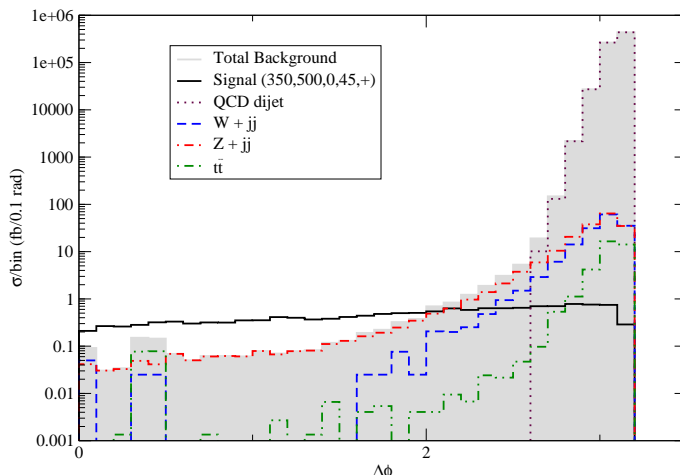


Figure 17: Distribution of $\Delta\phi(j_1, j_2)$ for dijet events with no identified leptons for the mSUGRA point $m_0 = 350$ GeV, $m_{1/2} = 500$ GeV, $A_0 = 0$ GeV, $\tan\beta = 45$ and $\mu > 0$ at $\sqrt{s} = 10$ TeV, along with corresponding distributions from various SM sources. We require that $E_T(j_1) + E_T(j_2) > 700$ GeV, but make no restriction on E_T^{miss} .

that for this analysis, we assume that it will be possible to identify the electron in $W + 2j$ events if $W \rightarrow e\nu$, so that such events can be efficiently vetoed.⁹

To extract the SUSY reach in the dijet channel, we scan over a large range of mSUGRA model points and find the optimal set of cuts, using:

- $n(\text{jets}) = 2$
- $E_T(j) \geq 50$ GeV
- $E_T(j_1) + E_T(j_2) \geq 100 - 1000$ GeV (in steps of 50 GeV)
- $\alpha > 0.05, 0.1 - 0.9$ (in steps of 0.1)
- $\Delta\phi(j_1, j_2) < 0.05, 0.3 - 3$ (in steps of 0.3)
- number of isolated leptons (μ or e), $n(\ell) = 0$

The optimal cuts are selected to maximize $S/\sqrt{B+S}$ and satisfy the discovery criteria defined at the beginning of Sec. 3. Because the important backgrounds all peak at large values of $\Delta\phi(j_1, j_2)$, the most effective cut is $\Delta\phi(j_1, j_2) \lesssim 2$ over most of the parameter space. Cutting further on α is then not usually required, so that $\alpha \gtrsim 0.05$ is generally preferred in order to maximize the signal. As expected, the optimal $E_T(j_1) + E_T(j_2)$ cut increases with $m_{1/2}$, but is essentially independent of m_0 for $m_0 \lesssim 450$ GeV.

Our results for the optimized reach in the dijet channel are shown in Fig. 18. We see that LHC experiments will begin to probe SUSY in this channel even with just 0.05 fb^{-1}

⁹We have also not shown backgrounds from $W + j$ or $Z + j$ production where the W and Z decay to taus that decay hadronically. Because of the $E_T(j_1) + E_T(j_2)$ cut, these backgrounds will be significant only for small values of α , and peak at large values of $\Delta\phi$, and will be efficiently removed by the same cuts that remove the much larger QCD background.

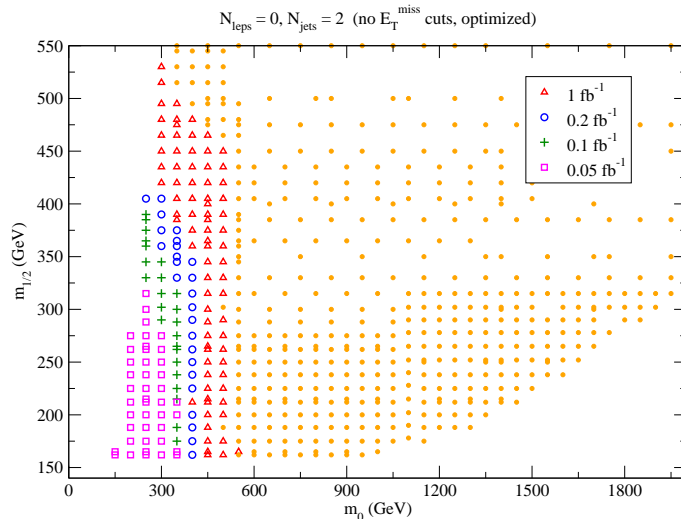


Figure 18: Optimized reach of LHC for mSUGRA at $\sqrt{s} = 10$ TeV via the RT-S dijet search, for various values of integrated luminosity. We assume that it will be possible to veto events with electrons or muons, but require no restriction on E_T^{miss} .

of integrated luminosity, if systematics are under control. With 1 fb^{-1} , LHC experiments should be able to probe to $m_{1/2}$ and m_0 values almost up to 500 GeV, corresponding to $m_{\tilde{q}} \sim m_{\tilde{g}}$ just over 1 TeV! In the white region at very small m_0 , the neutralino is not the LSP. As anticipated, the dijet search mainly probes the small m_0 region where squark pair production forms a significant part of the SUSY cross section.

4. Ultimate reach of the LHC utilizing E_T^{miss}

As the experiments accumulate data, the detectors will become better understood, and it will be possible to utilize both electrons and E_T^{miss} (well known to be a powerful discriminator between SUSY and SM events) in the analysis. Because of technical issues to do with re-training of the magnets, at present there is no clear projection for the time-line over which the energy of the LHC will be increased from the initial value of 7-10 TeV to its design value of 14 TeV. It is clear, however, that the energy increase will be staged [26]. The possibility that the design energy may not be attained for an extended period motivated us to study the impact of machine energy as well as integrated luminosity on the ultimate SUSY reach of the LHC. Toward this end, we delineate the LHC reach, including electrons and E_T^{miss} in the analysis of the signal, for $\sqrt{s} = 10$ and 14 TeV, for various values of integrated luminosity. Projections for intermediate energies may be obtained by interpolating between the reach for these two extreme values.

Before turning to the results, we draw attention to a potentially serious problem that arises when we try to make reach projections for integrated luminosities in the ab^{-1} range. In this case, SM backgrounds have to be limited to ab levels to make reliable projections for the observability of a signal (near the five event limit) with extremely hard cuts on jet and E_T^{miss} . In spite of the very large Monte Carlo background samples that we have

generated, we are forced to extrapolate our calculated backgrounds to obtain estimates of these backgrounds out to high values of E_T^{miss} for which our simulation becomes statistics-limited. For each process and for each set of jet and lepton cuts listed in Sec. 3.2.4, we extrapolate the background from the lower E_T^{miss} range to higher values of E_T^{miss} using an exponential fit whenever we have enough events in (at least three) low E_T^{miss} bins to allow a sensible extrapolation. In cases where this is not possible (mostly W and Z events with multiple jets and hard jet cuts) we do not extrapolate in this particular channel. However to avoid a huge under-estimation of this background when sensible extrapolation is not possible, we first check whether the non-extrapolated background level (in the channel in question) at low E_T^{miss} exceeds the corresponding extrapolated background cross-section (often dominantly from $t\bar{t}$ production which, we have checked, can be reliably extrapolated in most cases) by a factor ≥ 5 . If it does, we regard this set of cuts as *unsafe* (because the background that we could not extrapolate may indeed be too large) and exclude them from our optimization procedure.¹⁰ We recognize that this procedure may still underestimate the background at large E_T^{miss} in cases where the non-extrapolated W and Z backgrounds are below five times the total extrapolated one at low E_T^{miss} , but may become the dominant source at large E_T^{miss} , due to a flatter E_T^{miss} spectrum (when compared with the extrapolated ($t\bar{t}$) one), or simply because we did not obtain any $W/Z+j$ events in our simulation. We, therefore, regard the reach obtained after applying the procedure just described as the outer limit of the parameter plane that may be probed for the corresponding integrated luminosity and label it as oFIT (optimistic fit) in the reach plots below. We assume that the QCD background is smaller than the other backgrounds for high enough values of E_T^{miss} [28], so no extrapolation is done in this case. As already noted, it is frequently possible to extrapolate the $t\bar{t}$ background quite reliably, and extrapolation of backgrounds from multiple quark and vector boson production processes (if needed) is even more straightforward. Finally, we remark that even for these very large integrated luminosities, we have moderate control of the extrapolation of the SM backgrounds in the SS dilepton and $n_\ell \geq 3$ lepton channels, where $t\bar{t}$ production (or for higher lepton multiplicities, multiple vector boson processes) is the dominant background source and the W and Z backgrounds can be neglected. We regard our projection of the reach limited to these channels as conservative, and label it by cFIT in the plots to follow.

4.1 LHC reach using E_T^{miss} at $\sqrt{s} = 10$ TeV

We begin by reanalyzing the optimized reach of the LHC at $\sqrt{s} = 10$ TeV. In addition to the optimization over n_j , $E_T(j_1)$, $E_T(j_2)$ as in Sec. 3.2.4, we now include *all* leptons (e and μ) and also optimize over,

- $E_T^{\text{miss}} \geq 0 - 1500$ GeV (in steps of 100 GeV).
- $n(\ell) = 0, 1, 2, 3, 4, 5, 6$

¹⁰We have checked that dropping the set of cuts with the large W/Z background does not affect the reach that we obtain in any significant way. The optimization procedure picks out a different configuration where the W/Z background is smaller than the top background.

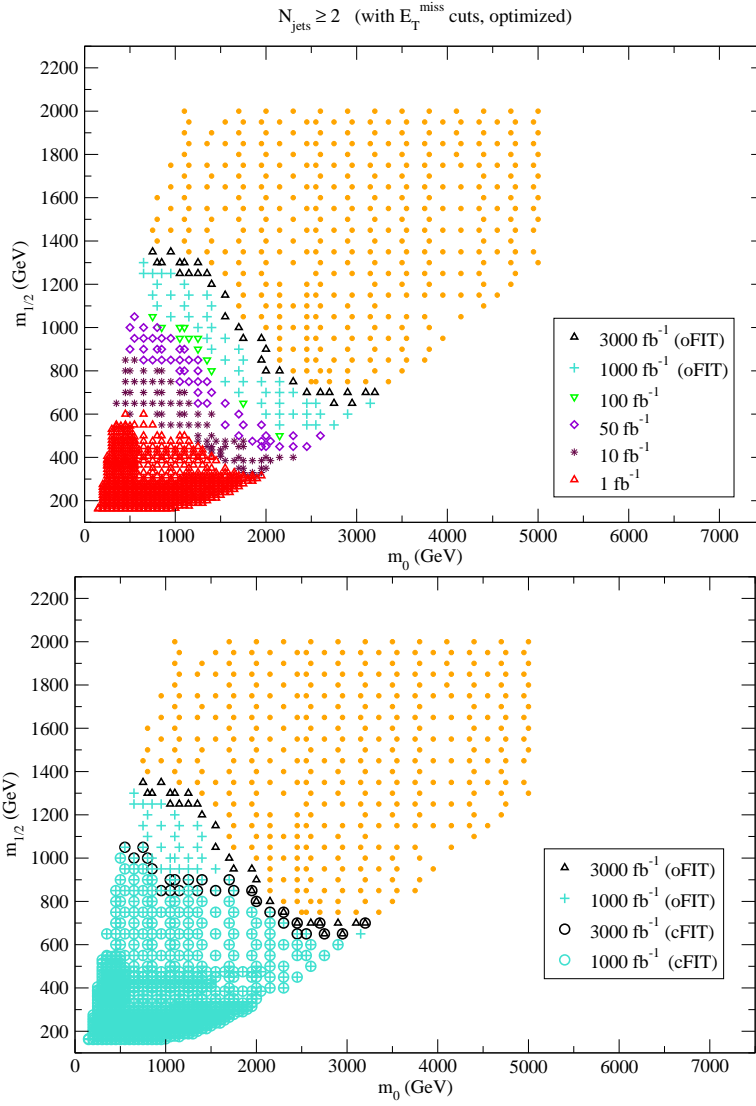


Figure 19: The upper frame shows the reach of LHC for mSUGRA at $\sqrt{s} = 10$ TeV using optimized cuts with $N(jet) \geq 2$, electron ID and E_T^{miss} for various values of integrated luminosities. For integrated luminosities of 1000 and 3000 fb^{-1} , the reach is obtained using the oFIT extrapolation procedure (discussed in the text) that likely underestimates the SM background, and leads to a correspondingly optimistic projection for the reach. The reach in the SS dilepton channel for 1000 and 3000 fb^{-1} (labeled cFIT) is shown by the circles in the lower frame, where the corresponding oFIT reach is also shown for comparison. We regard this as a conservative estimate of the SLHC reach. The fixed mSUGRA parameters are $A_0 = 0$, $\tan \beta = 45$ and $\mu > 0$.

where $\ell = \mu, e$. For the $n_\ell = 2$ OS dilepton signal, we continue to veto events with like-flavor, OS dilepton pairs with $75 \text{ GeV} \leq m(\ell^+\ell^-) \leq 105 \text{ GeV}$ or $m(\ell^+\ell^-) \leq 10 \text{ GeV}$.

Our results are shown in the top frame of Fig. 19. The reach in $m_{1/2}$ for low (high) m_0 extends to $m_{1/2} = 550$ (315) GeV for an integrated luminosity of 1 fb^{-1} , to be compared with 325 (250) GeV in Fig. 13. Thus, E_T^{miss} , together with help from electron ID leads

to about a 60% (25%) increase in the gluino mass reach if $m_{\tilde{q}} \sim m_{\tilde{g}}$ ($m_{\tilde{q}} \gg m_{\tilde{g}}$).¹¹ This same analysis gives projections for the machine reach with increased integrated luminosity. For integrated luminosities of 1, 10 and 100 fb⁻¹, the gluino mass reach (for $m_{\tilde{q}} \sim m_{\tilde{g}}$) is $\sim 1.4, 1.9, 2.3$ TeV. For integrated luminosities of 1000 and 3000 fb⁻¹, our projection for the *outer limit* of the LHC reach obtained using optimistic extrapolation of the SM backgrounds (oFIT) described above, extends out to 2.8 and 2.9 TeV, respectively. We caution that in this region our optimization procedure often selects out the $n_j = 2, n_\ell = 0$ or 1 topology with very hard jet and E_T^{miss} cuts, where the signal (for the 3000 fb⁻¹ case) is just 4 ab. At such low cross-sections the signal is likely termed “observable” only because the background from $W/Z + j$ production may be greatly underestimated. Aside from this, detector issues that will arise during LHC operation at very high instantaneous luminosity have not been included in this analysis, and may significantly reduce the 1000 fb⁻¹ and 3000 fb⁻¹ reach projections. The oFIT gluino mass reach drops to about 1.3 TeV (1.7 TeV) for an integrated luminosity of 100 (1000) fb⁻¹ if squarks are very heavy. We have checked that, after optimization, the signal almost always arises from gluino and squark production except at the largest values of m_0 where \tilde{W}_2 and \tilde{Z}_4 production contribute about a third of the signal. We repeat that, except possibly at the highest machine luminosities, the ultimate reach in $m_{1/2}$ in the HB/FP region will be about 15% higher than shown in this figure once b -jet tagging is utilized to enhance the signal over the SM background [17].¹²

To obtain a rough idea of how much the oFIT extrapolation may overestimate the reach, we compare the reach – shown by circles and labeled cFIT – that we obtain in the SS dilepton channel (for which we have moderate control on the SM backgrounds even for ab⁻¹ integrated luminosities) with the oFIT reach in the lower frame of Fig. 19. We see that for small values of m_0 , the envelope of even the black circles, roughly speaking, follows the 100 fb⁻¹ reach triangles in the upper frame, but for large m_0 gives a somewhat increased reach in $m_{1/2}$. Once again, except at the highest values of m_0 where \tilde{W}_2 and \tilde{Z}_4 production contributes up to a quarter, the signal (after optimization) is dominated by squark and gluino production. Modulo detector issues at high luminosity, we regard the cFIT reach shown in the figure as a conservative projection of the SLHC reach.

4.2 LHC reach with E_T^{miss} at $\sqrt{s} = 14$ TeV

We repeat the optimized cuts analysis that led to the reach in Fig. 19, for $\sqrt{s} = 14$ TeV. As for the 10 TeV case just discussed, we first show results using the oFIT to the backgrounds for SLHC integrated luminosities in the upper frame of Fig. 20. We see that the corresponding gluino mass reach (for $m_{\tilde{q}} \sim m_{\tilde{g}}$), shown in Table 1, extends to $m_{\tilde{g}} = (2.4, 3.1, 3.7)$ TeV for an integrated luminosity of (10, 100, 1000) fb⁻¹. We see that the

¹¹We have explicitly checked that the optimization mostly picks out the $n_\ell = 0$ channel, allowing us to conclude that the increased reach is essentially due to the availability of E_T^{miss} rather than of the electron signal.

¹²We mention that we have not imposed any cut on the transverse mass between the lepton and E_T^{miss} in our analysis of single lepton events. Since this cut is very efficient at removing backgrounds from $W + j$ and also $t\bar{t}$ events where just one W decays leptonically, it may be that with an $m_T(\ell, E_T^{\text{miss}}) \gtrsim 100$ GeV cut, a slightly bigger reach may be obtained in the single lepton channel. In the analysis presented here, the 0ℓ channel almost always yields the largest reach.

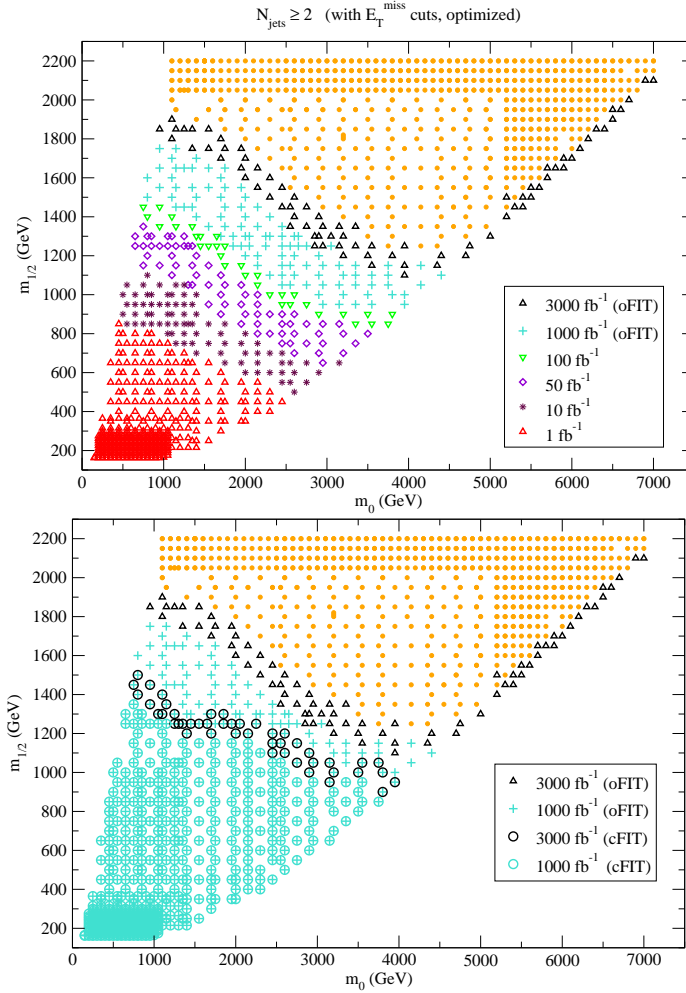


Figure 20: The upper frame shows the reach of LHC for mSUGRA at $\sqrt{s} = 14$ TeV using optimized cuts with $N(\text{jet}) \geq 2$, electron ID and E_T^{miss} for various values of integrated luminosities. For integrated luminosities of 1000 and 3000 fb^{-1} , the reach is obtained using the oFIT extrapolation procedure (discussed in the text) that likely underestimates the SM background, and leads to a correspondingly optimistic projection for the reach. The reach in the SS dilepton channel for 1000 and 3000 fb^{-1} (and labeled cFIT) is shown by the circles in the lower frame, where the corresponding oFIT reach is also shown for comparison. We regard this as a conservative estimate of the SLHC reach. The fixed mSUGRA parameters are $A_0 = 0$, $\tan \beta = 45$ and $\mu > 0$.

typical gain in the gluino mass reach due to the increased machine energy is a factor 1.3-1.4, *i.e.* this reach, roughly speaking, scales with the center-of-mass energy, and extends to over 3 TeV (4 TeV) for an integrated luminosity of 100 (3000) fb^{-1} . We have checked that at the highest $m_{1/2}$ and modest m_0 values for which we find an observable signal our optimization procedure again picks out the $n_j = 2$ channel with very hard jet and E_T^{miss} cuts with a signal cross section of ~ 2 ab, and for the reasons mentioned in Sec. 4.1, the oFIT reach shown is almost certainly an overestimate.

The most striking new feature in the upper frame is the appearance of a signal in the

HB/FP region for an integrated luminosity of 3000 fb^{-1} . We have checked that the signal in this region arises only from \widetilde{W}_2 and \widetilde{Z}_4 production, in the $n_j \geq 2$ channel with very hard jet and E_T^{miss} cuts. Even in the region near $m_0 \sim 4000 \text{ GeV}$ and $m_{1/2} = 1200 \text{ GeV}$ where the SLHC reach contours flatten out, electroweak-ino production accounts for about half the signal, whereas for yet lower values of m_0 , the signal originates essentially in gluino and squark events. The signal deep in the HB/FP region is just above the 5σ level with a cross-section of $\sim 5 \text{ ab}$ and, for fixed $m_{1/2}$, rapidly falls if m_0 is reduced because the mass gap between the wino parent and the higgsino LSP quickly reduces, softening the E_T^{miss} spectrum, concomitantly reducing the efficiency for the signal to pass the hard E_T^{miss} cut required to reduce the background. Indeed, it is very likely that we obtain the reach in the HB/FP region only because we get no background from $W/Z + j$ production in one (or more) of the many channels examined in the course of the optimization.

In the lower frame of Fig. 20 we show the corresponding reach in the SS dilepton channel. As in the previous figure, the cFIT circles denote points where the signal is observable in the SS dilepton channel. Except in the region at $m_{1/2} \sim 1 \text{ TeV}$ and $m_0 > 3 \text{ TeV}$ where about half the signal comes from wino production, the SS dilepton signal arises mostly from gluino and squark production. We also see that the HB/FP region entirely disappears. Since any signal in this region is most likely to come from \widetilde{W}_2 and \widetilde{Z}_4 production which yields SS dilepton events only if at least one final state lepton fails to be identified in the detector, we also checked that there is no observable signal in the $n_\ell \geq 3$ lepton channel, or for that matter in the inclusive SS and $n_\ell \geq 3$ event channels. We see that as in the $\sqrt{s} = 10 \text{ TeV}$ case, our more conservative projection for the reach is again close to the projected reach with 100 fb^{-1} shown in the upper frame of the figure.

5. Concluding remarks and summary

LHC experiments will soon probe particle collisions in a qualitatively new energy regime and, we hope, uncover new phenomena. In this paper, we assess the LHC reach for supersymmetric particles, both at the very early stages of LHC operation at the starting center-of-mass energy of 10 TeV and limited values of integrated luminosity ($0.1\text{-}1 \text{ fb}^{-1}$) when the detectors will not yet be completely understood and calibrated, as well as at later stages of LHC operation at $\sqrt{s} = 10$ and 14 TeV , again for several values of integrated luminosity extending up to the design value, and beyond into the super-LHC stage. To obtain these reach projections, we have used improved techniques described in Sec. 2 to calculate SM backgrounds from a large number of $2 \rightarrow n$ processes.

It has, however, often been stated that exploration of new physics (except for resonances that can be reconstructed as mass bumps) will only be possible after all the detectors systems are completely understood, and the ‘‘SM is rediscovered at the LHC’’. This dictum has been thought to be especially true for the discovery of supersymmetry¹³ since the experimental determination of E_T^{miss} , which is an essential element of the canonical SUSY

¹³The dictum applies equally well to a variety of proposals that address the mechanism of electroweak symmetry breaking and the stabilization of the electroweak scale and include a stable weakly interacting massive particle that escape detection in the experimental apparatus [31].

signal, truly does require a reliable identification and measurement of all high E_T electrons, muons, photons and jets in each event. This motivated us to examine the prospects for early sparticle detection without use of E_T^{miss} .

Since electron fakes from jets could be a serious issue in the early stages of operation, and since non-leptonic and single-muon signals will have large SM backgrounds, in Sec. 3 we focused on multi-muon signals from SUSY without any requirement on E_T^{miss} . We concluded that at the LHC start-up energy $\sqrt{s} = 10$ TeV, the OS dimuon channel (which has the highest rate of the multi-muon signals) offers the best prospects for the earliest detection of SUSY: even with very basic cuts and just 100 pb^{-1} of integrated luminosity, LHC experiments will probe significant portions of mSUGRA parameter space beyond the range of Tevatron experiments. The dimuons from the SUSY signal will have masses that tend to cluster close to, but below the expected mass edge at $m_{\tilde{Z}_2} - m_{\tilde{Z}_1}$. As more data are accumulated, the relatively background-free but rate-limited SS dimuon and trimuon channels become the more important, with the latter yielding the highest reach, with gluinos as heavy as 700 GeV being accessible with 1 fb^{-1} of data if $m_{\tilde{q}} \sim m_{\tilde{g}}$. This reach may be extended to 800 GeV using optimized cuts, though by the time such analyses can be performed, it is possible that reliable measurement of E_T^{miss} will also be available. We have also presented a number of muon distributions that serve to characterize the signal, and allow us to make at least a circumstantial case for its supersymmetric origin. In this connection, see especially the discussion of the low mass dimuon in trimuon events, and the distribution of the transverse plane opening angle for OS and SS dimuon events.

If squarks are light ($m_{\tilde{q}} \sim m_{\tilde{g}}$), LHC experiments will be able to probe squark and gluino production in the acollinear dijet channel (mostly from squark pair production with squarks decaying directly to the LSP), *without the use of E_T^{miss}* [16] out to masses of several hundred GeV with just 200 pb^{-1} of integrated luminosity, and to $\gtrsim 1$ TeV with 1 fb^{-1} . We conclude that within the mSUGRA framework, *if squarks and gluinos are in the few hundred GeV range, there could be a variety of multi-muon and jet signals that will be detectable in LHC experiments even during the first run* that is expected to accumulate up to $\sim 200 \text{ pb}^{-1}$ of integrated luminosity, despite the fact that the detectors may not be well enough understood to allow the use of E_T^{miss} or electron signals in these analyses.

In Sec. 4, we examined the ultimate reach of the LHC for various integrated luminosities, assuming that the detectors are fully understood. We show results for $\sqrt{s} = 10$ and 14 TeV in Fig. 19 and Fig. 20, respectively. These are succinctly summarized in Fig. 21 where, for integrated luminosities of 1000 and 3000 fb^{-1} , we have shown likely over-optimistic reach projections obtained using the oFIT extrapolation to estimate SM backgrounds with very hard cuts. We observe the following luminosity and energy scaling rules for the approximate sparticle reach (using optimistic oFIT projections) when $m_{\tilde{q}} \sim m_{\tilde{g}}$.

- The reach scales with machine energy, so that the gluino reach increases by about 40% between $\sqrt{s} = 10$ TeV and $\sqrt{s} = 14$ TeV.
- At $\sqrt{s} = 10$ (14) TeV, every order of magnitude increase in luminosity gives an increase in reach of ~ 400 (~ 600) GeV. We caution though that the oFIT projections

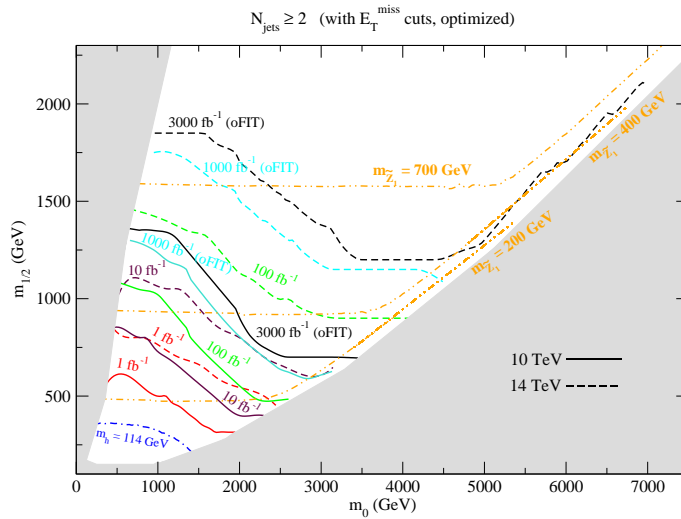


Figure 21: The ultimate SUSY reach of LHC within the mSUGRA framework for $\sqrt{s} = 10$ TeV (solid) and $\sqrt{s} = 14$ TeV (dashed) for various values of integrated luminosities. For integrated luminosities of 1000 and 3000 fb^{-1} , we have shown our (over)-optimistic projections obtained using the oFIT procedure that tends to underestimate SM backgrounds. A conservative projection for the corresponding reach essentially follows the 100 fb^{-1} contour. The fixed mSUGRA parameters are $A_0 = 0$, $\tan \beta = 45$ and $\mu > 0$. Isomass contours for the LSP (double dot-dashed) and for a 114 GeV light Higgs scalar (dot-dashed) are also shown. The shaded areas are excluded either because the neutralino is not the LSP, or electroweak symmetry breaking is not correctly obtained.

very likely over-estimate the reach for integrated luminosities at the ab^{-1} level, and the growth of the reach with luminosity may well slow down after $\sim 100 \text{fb}^{-1}$.

The situation is more complicated for very large values of m_0 where signals from electroweak $\widetilde{W}_2 \widetilde{W}_2$ and $\widetilde{W}_2 \widetilde{Z}_4$ production appear to yield an increased reach in the HB/FP region at $\sqrt{s} = 14$ TeV and ab^{-1} values of integrated luminosity as seen by the up-turn of the black dashed reach contour in Fig. 21. As mentioned earlier, it is very likely that the oFIT procedure seriously under-estimates the background from $W/Z + j$ production, and that there is really no reach in the HB/FP region. More generally, barring clever new strategies (for instance, using gauge boson polarizations) to enhance the new physics signal, we believe that the oFIT contours yield over-optimistic projections over most of the $m_0 - m_{1/2}$ plane.

Fig. 22 presents a snapshot of the ultimate gluino mass reach of the LHC, with $\sqrt{s} = 10$ (solid histogram) and 14 TeV (dashed histogram), for several values of integrated luminosity. The hatched portions of the bar show the LHC reach in terms of $m_{\tilde{g}}$. The height of the lower hatched portion (bottom-right to top-left hatching) of each bar shows the value of $m_{\tilde{g}}$ up to which discovery of gluinos is guaranteed at the LHC irrespective of the squark mass, while the height of the upper hatched part (top-right to bottom-left hatching) bars correspond to the maximum value of $m_{\tilde{g}}$ that LHC experiments will be able to probe for some value of m_0 (usually small), where typically $m_{\tilde{g}} \sim m_{\tilde{q}}$. For integrated luminosities $\geq 1 \text{ab}^{-1}$, the reach shown is obtained from the likely over-optimistic oFIT procedure to

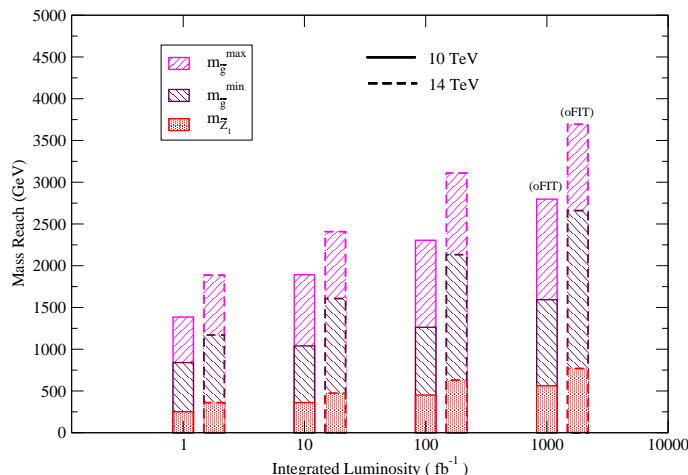


Figure 22: The ultimate reach of the LHC at $\sqrt{s} = 10$ TeV (solid) and $\sqrt{s} = 14$ TeV (dashed) in terms of the gluino and the LSP masses within the mSUGRA framework, for several values of the integrated luminosity. Results for the 1000 fb^{-1} case are obtained using the oFIT procedure to extrapolate the background. A conservative analysis would give results close to those for 100 fb^{-1} . The heights of the lower (top-left to bottom-right) hatched bars show the value of $m_{\tilde{g}}$ up to which gluinos are guaranteed to be detectable at the LHC regardless of squark masses, while the heights of the upper (top-right to bottom-left) hatched bars show the greatest gluino mass that may be accessible, usually when $m_{\tilde{q}} \sim m_{\tilde{g}}$. The dotted bars show the range of the lightest neutralino mass over the part of mSUGRA parameter space for which there is an observable SUSY signal at the LHC.

extrapolate the background. Finally, the range of the lightest neutralino mass over the region of mSUGRA parameter space where LHC experiments will be able to detect a SUSY signal is shown by the red-dotted bars in the figure. Comparing with earlier studies [32], we see that there will be detectable signals in the next round of direct dark matter searches – XENON, LUX with ~ 100 kg of noble liquids, or superCDMS (25kg) – over the entire \tilde{Z}_1 mass range in the figure, and also at IceCube if $m_{\tilde{Z}_1} \lesssim 550 - 600$ GeV, if parameters are in the HB/FP region, where the neutralino composition is adjusted to give the measured amount of dark matter. Instead, for a bino-like \tilde{Z}_1 , direct searches with ton-sized detectors will be sensitive to \tilde{Z}_1 masses up to about 300 GeV. It is exciting that if supersymmetry is realized as in the mSUGRA framework (or one of its variants with non-universal parameters), we expect observable signals not only at the LHC, but also in a completely different program of experiments unrelated to accelerator particle physics.

Acknowledgments

We thank M. Drees for many very helpful comments on an early version of the manuscript. VB thanks the Aspen Center for Physics for hospitality. This research was supported in part by the U.S. Department of Energy, by the Fulbright Program and CAPES (Brazilian Federal Agency for Post-Graduate Education).

References

- [1] From analysis of the LEP Electroweak Working Group, <http://lepewwg.web.cern.ch/LEPEWWG/>
- [2] For reviews of SUSY, see H. Baer and X. Tata, *Weak Scale Supersymmetry: From Superfields to Scattering Events*, (Cambridge University Press, 2006); M. Drees, R. Godbole and P. Roy, *Theory and Phenomenology of Sparticles*, (World Scientific, 2004); P. Binetruy, *Supersymmetry* (Oxford University Press, 2006); S. P. Martin, hep-ph/9709356.
- [3] For perspective on SM background to SUSY signals, see *e.g.* H. Baer, V. Barger and G. Shaughnessy, *Phys. Rev. D* **78** (2008) 095009; M. Mangano, *Eur. Phys. J. C* **59** (2009) 373.
- [4] H. Baer, C. H. Chen, F. Paige and X. Tata, *Phys. Rev. D* **52** (1995) 2746 and *Phys. Rev. D* **53** (1996) 6241; H. Baer, C. H. Chen, M. Drees, F. Paige and X. Tata, *Phys. Rev. D* **59** (1999) 055014 H. Baer, C. Balázs, A. Belyaev, T. Krupovnickas and X. Tata, *J. High Energy Phys.* **0306** (2003) 054; see also, S. Abdullin and F. Charles, *Nucl. Phys. B* **547** (1999) 60; S. Abdullin *et al.* (CMS Collaboration), *J. Phys. G* **28** (2002) 469 [hep-ph/9806366]; B. Allanach, J. Hetherington, A. Parker and B. Webber, *J. High Energy Phys.* **08** (2000) 017.
- [5] A. Chamseddine, R. Arnowitt and P. Nath, *Phys. Rev. Lett.* **49**, 970 (1982); R. Barbieri, S. Ferrara and C. Savoy, *Phys. Lett. B* **119**, 343 (1982); N. Ohta, *Prog. Theor. Phys.* **70**, 542 (1983); L. Hall, J. Lykken and S. Weinberg, *Phys. Rev. D* **27**, 2359 (1983).
- [6] H. Baer, J. K. Mizukoshi and X. Tata, *Phys. Lett. B* **488** (2000) 367; A. J. Barr, C. G. Lester, A. Parker, B. Allanach and P. Richardson, *J. High Energy Phys.* **0303** (2003) 045.
- [7] H. Baer, E-K. Park, X. Tata and T. Wang, *J. High Energy Phys.* **0706** (2007) 033.
- [8] H. Baer, P. Mercadante, F. Paige, X. Tata and Y. Wang, *Phys. Lett. B* **435** (1998) 109; H. Baer, P. Mercadante, X. Tata and Y. Wang, *Phys. Rev. D* **62** (2000) 095007.
- [9] H. Baer, A. Belyaev, T. Krupovnickas and X. Tata, *Phys. Rev. D* **65** (2002) 075024.
- [10] H. Baer, C. H. Chen and X. Tata, *Phys. Rev. D* **55** (1997) 1466.
- [11] H. Baer, J. Ellis, G. Gelmini, D. V. Nanopoulos and X. Tata, *Phys. Lett. B* **161** (1985) 175; G. Gamberini, *Z. Physik C* **30** (1986) 605; H. Baer, V. Barger, D. Karatas and X. Tata, *Phys. Rev. D* **36** (1987) 96.
- [12] H. Baer, X. Tata and J. Woodside, *Phys. Rev. D* **45** (1992) 142.
- [13] D. Green, hep-ph/0601038 (2006); see also, F. Gianotti and M. Mangano, hep-ph/0504221 (2005); J. Hubisz, J. Lykken, M. Pierini and M. Spiropulu, *Phys. Rev. D* **78** (2008) 075008; M. Mangano, *Int. J. Mod. Phys. A* **23** (2008) 3833; J. Lykken and M. Spiropulu, *Int. J. Mod. Phys. A* **23** (2008) 3441
- [14] H. Baer, H. Prosper and H. Summy, *Phys. Rev. D* **77** (2008) 055017.
- [15] H. Baer, A. Lessa and H. Summy, *Phys. Lett. B* **674** (2009) 49.
- [16] L. Randall and D. Tucker-Smith, *Phys. Rev. Lett.* **101** (2008) 221803.
- [17] U. Chattopadhyay, A. Datta, A. Datta, A. Datta and D. P. Roy, *Phys. Lett. B* **493** (2000) 127; P. G. Mercadante, J. K. Mizukoshi and X. Tata, *Phys. Rev. D* **72** (2005) 035009; S. P. Das, A. Datta, M. Guchait, M. Maity and S. Mukherji, *Eur. Phys. J. C* **54** (2008) 645; R. Kadala, P. G. Mercadante, J. K. Mizukoshi and X. Tata, *Eur. Phys. J. C* **56** (2008) 511.

- [18] M. Mangano, M. Moretti, F. Piccinini, R. Pittau and A. Polosa, *J. High Energy Phys.* **0307** (2003) 001.
- [19] F. Maltoni and T. Stelzer, *J. High Energy Phys.* **0302** (2003) 027.
- [20] B. Allanach *et al.*, [hep-ph/0202233](https://arxiv.org/abs/hep-ph/0202233) (2006).
- [21] H. Baer, A. Box and H. Summy, [arXiv:0906.2595](https://arxiv.org/abs/0906.2595) (2009).
- [22] MCFM, by J. Campbell and R. K. Ellis. See R. K. Ellis, *Nucl. Phys. Proc. Suppl.* **160** (2006) 170.
- [23] T. Sjostrand, S. Mrenna and P. Skands, *J. High Energy Phys.* **0605** (2006) 026.
- [24] ISAJET, by H. Baer, F. Paige, S. Protopopescu and X. Tata, [hep-ph/0312045](https://arxiv.org/abs/hep-ph/0312045); see also H. Baer, J. Ferrandis, S. Kraml and W. Porod, *Phys. Rev. D* **73** (2006) 015010.
- [25] F. Paige, presented at PPC 2009, Third International Workshop on the Interconnections between Particle Physics and Cosmology, Norman, Oklahoma, (May 2009).
- [26] P. Jenni, plenary talk at SUSY 09, *17th International Conference on Supersymmetry and the Unification of Fundamental Interactions*, Northeastern University, Boston, MA, (June 2009).
- [27] H. Baer, K. Hagiwara and X. Tata, *Phys. Rev. D* **35** (1987) 1598; H. Baer, D. Dzialo-Karatas and X. Tata, *Phys. Rev. D* **42** (1990) 2259; H. Baer, C. Kao and X. Tata, *Phys. Rev. D* **48** (1993) 5175; H. Baer, C. H. Chen, F. Paige and X. Tata, *Phys. Rev. D* **50** (1994) 4508; I. Hinchliffe *et al.* *Phys. Rev. D* **55** (1997) 5520; H. Bachacou, I. Hinchliffe and F. Paige, *Phys. Rev. D* **62** (2000) 015009; See also, ATLAS collaboration, *Atlas Physics and Detector Performance Technical Design Report LHCC 99-14/15*, and *Expected Performance of the ATLAS Experiment: Detector, Trigger and Physics*, CERN-OPEN-2008-020; CMS Collaboration, *Physics Technical Design Report, V. II*, CERN/LHCC 2006-021.
- [28] M. Narain, UC Davis Seminar, <http://particle.physics.ucdavis.edu/seminars/data/media/2009/apr/narain.pdf>; S. Padhi, http://www-wisconsin.cern.ch/physics/files/BSM_padhi_181206.pdf.
- [29] V. Abazov *et al.* (DØCollaboration) *Phys. Lett. B* **660** (2008) 449; T. Aaltonen *et al.* (CDF Collaboration) *Phys. Rev. Lett.* **102** (2009) 121801.
- [30] H. Baer, A. Belyaev, T. Krupovnickas and X. Tata, *J. High Energy Phys.* **0402** (2004) 007, and H. Baer, T. Krupovnickas and X. Tata, *J. High Energy Phys.* **0406** (2004) 041.
- [31] H. Baer, lectures at TASI 2008, [arXiv:0901.4732](https://arxiv.org/abs/0901.4732) (2009).
- [32] See, *e.g.* H. Baer, A. Mustafayev, E-K. Park and X. Tata, *J. High Energy Phys.* **0805** (2008) 058; V. Barger, W.-Y. Keung and G. Shaughnessy, *Phys. Rev. D* **78** (2008) 056007.